

Mutations in *ANXA11* cause familial and sporadic amyotrophic lateral sclerosis

Bradley N Smith^{1†}, Simon Topp^{1†}, Claudia Fallini^{2†}, Hideki Shibata^{3†}, Han-Jou Chen^{1†}, Claire Troakes¹, Andrew King¹, Nicola Ticozzi⁴, Kevin P. Kenna², Akane Sato³, Athina Soragia-Gkazi¹, Jack Miller¹, Caroline Vance¹, Chun-Hao Wong¹, Martina de Majo¹, Wejdan Kattuah¹, Jacqueline C Mitchell¹, Emma L Scotter⁵, Nicholas Parkin⁶, Peter C. Sapp², Matthew Nolan¹, Peter J Nestor⁷, Michael Simpson⁸, Frank Baas⁹, Vianney de Jong JM⁹, Anneloor LMA ten Asbroek⁹, Alberto Garcia Redondo¹⁰, Jesús Esteban-Pérez¹⁰, José Luis Muñoz-Blanco¹¹ Cinzia Tiloca⁴, Federico Verde⁴, Stefano Duga¹², Nigel Leigh¹³, Pall H¹⁴, Karen E. Morrison¹⁵, Ammar Al-Chalabi¹, Pamela J. Shaw¹⁶, Janine Kirby¹⁶, Martin R. Turner¹⁷, Kevin Talbot¹⁷, Orla Hardiman¹⁸, Jonathan D. Glass¹⁹, Jacqueline de Belleruche²⁰, Masatoshi Maki⁴, Steve Moss²¹, Christopher Miller¹, Cinzia Gellera²², Antonia Ratti⁴, Safa Al-Sarraj¹, Robert H Brown Jr², Vincenzo Silani^{4*}, John E Landers^{3*}, Christopher E Shaw^{1*}

†* These authors made equal contributions to the manuscript

1. Maurice Wohl Clinical Neuroscience Institute, Institute of Psychiatry, Psychology and Neuroscience, King's College London, 125 Coldharbour Lane, Camberwell, SE5 9NU, London, UK.
2. Department of Neurology, University of Massachusetts Medical School, Worcester, Massachusetts 01605, USA.
3. Department of Applied Molecular Biosciences, Graduate School of Bioagricultural Sciences, Nagoya University, Furo-cho, Chikusa-ku, Nagoya 464-8601, Japan.
4. Department of Neurology and Laboratory of Neuroscience, IRCCS Istituto Auxologico Italiano, Milan 20149, Italy.
5. The Centre for Brain Research, Faculty of Medical and Health Sciences, University of Auckland, 85 Park Road, Grafton, Auckland, New Zealand.
6. Molecular Genetics, Viapath, 5th Floor, Tower Wing, Guy's Hospital, Kings College London, London Bridge, SE1 9RT.
7. German Center for Neurodegenerative Diseases, Leipziger Str. 44, 39120 Magdeburg, Germany.
8. Medical & Molecular Genetics, Division of Genetics and Molecular Medicine, Guys Tower, Kings College London, London Bridge, SE1 9RT.
9. University of Amsterdam, Academic Medical Center, PO Box 22700, 1100DE, Amsterdam, The Netherlands.
10. Unidad de ELA, Instituto de Investigación Hospital 12 de Octubre de Madrid, SERMAS, and Centro de Investigación Biomédica en Red de Enfermedades Raras (CIBERER U-723), Madrid, Spain.
11. Unidad de ELA, Instituto de Investigación Hospital Gregorio Marañón de Madrid, SERMAS, Spain.
12. Department of Biomedical Sciences, Humanitas University, Milan Italy.
13. Trafford Centre for Medical Research, Brighton & Sussex Medical School, BN1 9RY
14. School of Clinical and Experimental Medicine, College of Medical and Dental Sciences, The University of Birmingham, Birmingham, UK.

15. School of Clinical and Experimental Medicine, College of Medical and Dental Sciences, University of Birmingham, UK, Queen Elizabeth Hospital, University Hospitals Birmingham NHS Foundation Trust UK.
16. Sheffield Institute for Translational Neuroscience, University of Sheffield, Sheffield, UK.
17. Nuffield Department of Clinical Neurosciences, John Radcliffe Hospital, Oxford, UK.
18. Academic Unit of Neurology, Trinity Biomedical Sciences Institute, Trinity College Dublin, Dublin, Republic of Ireland.
19. Department of Neurology, Center for Neurodegenerative Disease, Emory University School of Medicine, Atlanta, Georgia 30322, USA.
20. Neurogenetics Group, Division of Brain Sciences, Imperial College London, Hammersmith Hospital Campus, Burlington Danes Building, Du Cane Road, London, W12 0NN.
21. Institute of Ophthalmology, University College London, 1-43 Bath Street, EC1V 9EL, London, UK.
22. Unit of Genetics of Neurodegenerative and Metabolic Diseases, Fondazione IRCCS Istituto Neurologico 'Carlo Besta', 20133 Milan, Italy.

Corresponding author: Bradley N Smith, Maurice Wohl Clinical Neuroscience Institute, Institute of Psychiatry, Psychology and Neuroscience, King's College London, 125 Coldharbour Lane, Camberwell, SE5 9NU, London, UK. (T) +44 207 848 0974, email: bradley.smith@kcl.ac.uk

Abstract

Amyotrophic Lateral sclerosis (ALS) is a fatal neurodegenerative disorder. We screened 608 familial ALS exomes and identified 6 novel, or extremely rare, *Annexin A11* mutations in 12 individuals. The novel p.D40G mutation which was absent from >60,000 exomes; segregated with disease in two kindreds, was present in two unrelated cases and all carriers shared a common haplotype. Annexin A11-positive aggregates were abundant in spinal motor neurons and hippocampal axons in a D40G patient. Transfected cells expressing p.D40G and other N-terminal mutations had altered calcyclin binding while the p.R235Q mutant formed toxic, insoluble aggregates. *Annexin A11* mutations accounted for ~1.2% of familial and ~1.7% of sporadic cases. Mutations in *Annexin A11* highlight the role of defective cellular trafficking in the pathogenesis of ALS.

Introduction

Gene hunting in rare Mendelian disorders has been transformed by exome sequencing, particularly for autosomal recessive disorders [1]. This approach is also attractive for late-onset autosomal dominant syndromes with short disease durations, such as Amyotrophic Lateral Sclerosis (ALS), in which DNA from multiple affected individuals in the same kindred is rare. ALS has a life-time risk of 1/400 and is characterized by degeneration of brain and spinal cord motor neurons resulting in progressive paralysis and death within an average of 3 years [2]. 10% of cases are familial (FALS) and a causative gene mutation can be identified in ~60% of European kindreds [3]. Mutations in the same genes account for ~10% of sporadic ALS cases reflecting incomplete penetrance. Non-synonymous mutations in *SOD1*, *TARDBP*, *FUS* and an intronic hexanucleotide repeat expansion in *C9ORF72* account for ~20% of ALS cases and the other genes for ~1-3% [4]. Exome sequencing has identified six ALS genes where mutations segregate with disease (*VCP*, *PFN1*, *MATR3* and *CHCHD10*) or by genetic burden analysis (*TUBA4A* and *TBK1*) [5-11]. Here we analysed FALS exomes to

identify common founder non-synonymous variants present in multiple unrelated index cases to identify candidate ALS genes [12-14].

Exome sequencing, filtering and gene identification

The exomes of 403 FALS index cases without mutations in known ALS genes were analyzed in an unbiased fashion. Successive filtering steps were used to identify single nucleotide changes present in 2 or more FALS cases but absent in the exomes of ~60,000 individuals in publicly available databases (1000 Genomes, NHLBI GO Exome Sequencing Project (ESP), UK 10K, ExAC and 672 In-house UK exome controls, see Supplementary Information). Sixty novel heterozygous missense, nonsense or splice changing variants were shared by at least two index cases (Supplementary Table 1). As proof of methodology, the same approach was applied to 58 exomes with known mutations, which identified 6 mutations in three known ALS genes (*SOD1*, *TARDBP* or *FUS*).

We then analyzed an independent replication cohort of 205 index FALS cases (and 47 where the mutation was known), which confirmed two of the novel variants in the discovery cohort and the total number of shared novel variants rose to 95 (Supplementary Table 1). The top novel variant was p.D40G (c.119A>G) in *ANXA11* (*Annexin A11*, Refseq NM_145869) that, in addition to being found three times, also satisfied segregation criteria. Sanger sequencing of 18 family members confirmed the presence of the mutation in another affected individual from each of two multi-generational British kindreds in the discovery cohort (Figs 1A-B). Four unaffected individuals also carried the mutation but three of these were in their forties and the average age of disease onset in these kindreds was 72 years. In the replicate cohort one Italian FALS index case also carried the D40G variant. Sanger sequencing a cohort of 180 British sporadic ALS cases (SALS) identified one further p.D40G carrier. All five British D40G carriers share a common haplotype on the disease allele defined by 8 SNPs and 2 microsatellites spanning the locus confirming a common founder (Supplementary Figure 1).

Additional *ANXA11* variants identified in the discovery FALS cohort were two unrelated individuals carrying a c.112G>A, p.G38R variant (rs81930608) that was absent from local UK and Italian exome controls (n=4505). Although the p.G38R variant is present in 6/55261 ExAC exomes it is still significantly associated with FALS in our cohort (p=0.007, 2-tailed Fishers exact test). In the replication cohort, novel p.G175R (c.523G>A) and p.R346C (c.1036C>T) variants were detected in two index cases. The p.G175R was also present in an affected sibling with ALS (Fig 1C) confirming segregation with disease. All coding exons of *ANXA11* were Sanger sequenced in an additional 180 British SALS cases. One individual carried a novel p.R235Q (c.704G.A) change and another case a p.G189E (c.566G>A) variant which is present in 14/33140 in European cases in ExAC (p=0.05) but is also present in one SALS case in the Biogen database ALSdB (<http://chgv.org/alsdb/index.jsp>). All but one of the *ANXA11* variants identified here are predicted to be damaging by Polyphen (see Supplementary Table 2).

Annexin A11 is a widely expressed, calcium-dependent phospholipid-binding protein (505AA, 56kDa) that belongs to the larger annexin family of 12 members (Interpro ID IPR001464). Each family member has four annexin domains many of which can complex a calcium ion facilitating binding to anionic cell membranes. Four of the six mutations in Annexin A11 cluster within the long N Terminus with p.G38R and p.D40G representing a mutation hotspot, implying that this region has functional importance. All mutation positions are completely conserved in mammals and those in the annexin domains are also conserved in all currently sequenced birds, amphibians and reptiles (Fig 1D).

Clinical Features and Neuropathology

All patients with *ANXA11* mutations had late disease onset (average 67 yrs) with a classical ALS phenotype without features of dementia (Supplementary Table 3). Five of six patients carrying the p.D40G variant had bulbar onset. Post mortem tissue was available from a SALS case carrying the p.D40G variant showing classical pathological features of ALS with a unique feature of large Annexin A11 immunoreactive inclusions that were absent from other ALS cases or controls (Fig 2). Spinal cord sections revealed marked neuronal loss within the anterior horns. There was marked myelin pallor and astrogliosis in the anterior and lateral corticospinal tracts. Many surviving motor neurons contained cytoplasmic inclusions positive for p62 and phospho-TDP-43 (Figure 2 A). Phospho-TDP-43 inclusions were also found in the medulla, temporal neocortex and hippocampus (data not shown). Annexin A11 staining of spinal cord sections showed numerous neuronal cytoplasmic inclusions (NCIs) in the perikaryon and proximal axon (Figures 2B-E). These included large-caliber tubular-shaped structures (Fig 2C-D) as well as skein-like (2B), filamentous and more complex basket-like inclusions (2E). Annexin positive NCIs were also evident in small numbers in the motor cortex, dentate gyrus of the hippocampus and temporal neocortex sometimes accompanied by abundant torpedo-like neuritic structures in the neuropil (Figure 2F). Staining for the amyloid precursor protein, Neurofilament, and β 3 tubulin was negative. SALS devoid of known mutations and controls were negative for annexin NCIs (Fig 2G-H). Double fluorescent labelling of phospho-TDP-43 and annexin A11 showed no evidence of co-localization (Fig 2I and J). Some annexin A11 positive aggregates were ubiquitinated (Figs 2K and L).

Functional studies

In order to understand the functional significance of these variants we undertook a series of cellular studies of mutations identified in our discovery exome set. We generated *ANXA11*^{WT}, *ANXA11*^{G38R}, *ANXA11*^{D40G} and *ANXA11*^{R235Q} tagged with hemagglutinin (HA) or GFP at the C-terminus. Constructs were expressed in mouse primary motor neurons (PMNs), human embryonic kidney 293 (HEK) and SH-SY5Y neuroblastoma cells. PMNs transfected with *ANXA11*-HA^{WT} constructs showed nuclear and cytoplasmic localization. In the cytoplasm *ANXA11* was present in larger vesicle-like structures, smaller foci structures (classified by size, see Supplementary Methods) and diffusely distributed throughout the soma, axons and dendrites (Fig 3A). Apart from *ANXA11*-HA^{R235Q}, which was elevated in the cytoplasm, there was no evidence that the other mutations affected the distribution between the nucleus and cytoplasm (Fig 3B) [15]. The *ANXA11*-HA^{R235Q} mutant appeared to aggregate into foci, was never associated with the vesicular-like structures and diffuse staining was absent ($p < 0.001$) (Fig 3C). *ANXA11*-HA^{D40G} had a similar pattern to WT but *ANXA11*-HA^{G38R} displayed significantly less association with the vesicle-like structures ($p = 0.005$). *ANXA11*-GFP^{R235Q} expression in HEK cells showed marked aggregation into ubiquitin and p62 positive inclusions (Supplementary Figure 2) with high molecular weight species on western blot that were insoluble (Supplementary Figure 3) ($p = 0.007$). SH-SY5Y cells transfected with *ANXA11*-GFP demonstrated the *ANXA11*-GFP^{R235Q} mutant to be toxic but not the other mutants ($p = 0.0001$) (Supplementary Figure 4). We also investigated whether *ANXA11* is self-interacting by co-transfecting SH-SY5Y cells with either *ANXA11*-GFP^{WT} and *ANXA11*-HA^{WT} or *ANXA11*-GFP^{R235Q} and *ANXA11*-HA^{WT} (Fig 3D). The merge of WT-HA and WT-GFP showed nuclear and diffuse cytoplasmic staining as expected, however *ANXA11*-GFP^{R235Q} cytoplasmic puncta and WT-HA did co-localize. This suggests mutant *ANXA11* may act to recruit and sequester WT *ANXA11*, potentially in a dominant negative manner.

Next we sought to determine whether there was an interaction between TDP-43 and Annexin A11. PMNs were cotransfected with the C-terminal fragment of TDP-43 (AA 208-

414) tagged with GFP and each of the ANXA11-HA variants. The ANXA11-HA^{R235Q} aggregates robustly colocalised with CTF-TDP-43-GFP four days post-transfection (Fig 4E). Furthermore, vesicle-like structures containing the ANXA11-HA^{D40G} mutation appeared to significantly engulf TDP-43 aggregates that were not seen for the other mutations.

N-terminal mutants disrupt binding of ANXA11 to Calcyclin

Because residues 50-62 in Annexin A11 bind calyculin (encoded by S100A6) and are close to the mutants G38R and D40G we sought evidence for any effect on their interaction. Calyculin is a 10kDa protein that contains 2EF-hand calcium-binding motifs [16]. Alignment of all mammalian Annexin A11 orthologue sequences predicted that residues 38-45 and 50-60 form dual amphipathic helices known to mediate calcium-dependent protein-membrane interactions [17] (Supplementary Figure 5A). Annexin A1 has a similar dual amphipathic helix structure that in the absence of calcium is embedded within the annexin core but is released on calcium activation and facilitates its binding to S100A11 [18, 19] (Sup Fig 5B-C). Using Jpred4 software the Annexin A11 G38R variant is predicted to create a new beta-sheet while D40G is predicted to severely reduce formation of the first amphipathic helix, thus both of these mutants may disrupt calyculin binding but in different ways (Sup Fig 5D).

In order to assess the effects of mutations in Annexin A11 on calyculin binding we performed binding assays of ANXA11-GFP^{WT} and the ANXA11^{G38R, D40G, G189E and R235Q} mutants using a previously published *in-vitro* immuno-precipitation (IP) assay [20]. In brief, FLAG- Calyculin and ANXA11-GFP WT and mutant constructs were transfected into HEK cells, lysates were mixed and activated with calcium, immunoprecipitation (IP) was performed with anti-FLAG antibody and the resulting western blot probed for GFP. As expected WT GFP co-immunoprecipitated with calyculin, that confirmed calyculin–Annexin A11 binding. ANXA11-GFP^{D40G} severely disrupted calyculin binding, as did ANXA11-GFP^{G189E} and ANXA11-GFP^{R235Q} mutants (Figure 4A). ANXA11-GFP^{G38R} binding however was markedly increased compared to WT. Arginine is polar thus the p.G38R change could enhance the hydrophilic properties of the amphipathic helix that may explain enhanced calyculin binding. D40G, on the contrary is a charged to hydrophobic modification that could account for reduced calyculin interaction. No differences were observed in ANXA11 binding to other partners ALG2 and Sorcin (Supplementary Figure 6).

IHC on spinal cord sections from the ALS patient carrying the D40G mutation were stained with anti-calyculin antibody. Although there was no observable difference in neuronal staining between the ALS case and controls very high levels of calyculin expression were detected in the cytoplasm of astrocytes in the lateral corticospinal tracts compared to controls (Figs 4Bi-iv). This is not a mutation-specific event as elevated calyculin expression was also seen in sporadic ALS cases without known ALS gene mutations (Figs 4Bv-vi). Increased expression of calyculin in astrocytes of the corticospinal tract has previously been reported in sporadic ALS cases as well as SOD1^{G93A} transgenic mice [21, 22].

We also explored the impact of calyculin interaction on Annexin A11 solubility. FLAG-CACY^{WT} was co-transfected with ANXA11-GFP^{WT} or ANXA11-GFP^{R235Q} in HEK cells and the subcellular distribution assessed by immunocytochemistry and solubility by western blot. Remarkably, the increase in calyculin expression reduced levels of soluble WT and R235Q but it completely cleared insoluble ANXA11-GFP^{R235Q} (Fig4C). This suggests that increasing calyculin may inhibit ANXA11 expression or enhance ANXA11 clearance via a degradation pathway. Treating the cells with the ubiquitin proteasome inhibitor MG132 treatment for 24hrs restored ANXA11^{R235Q} insolubility.

Discussion

Using a stringent filtering strategy on large-scale FALS index case exome data we identified a non-synonymous mutation, D40G in Annexin A11 that segregates with disease in two large UK families and in two replicate FALS and SALS cohorts but is absent from >60,000 exomes. The G175R mutation segregated with disease in one kindred and several other *ANXA11* mutations were associated with ALS. The clinical phenotype was of late-onset classical ALS but 4 of 5 D40G cases had bulbar onset disease. Post mortem tissue from a D40G ALS case displayed abundant Annexin A11-positive aggregates within motor neurons in spinal cord and neurons and neuropil in the neocortex and hippocampus in addition to the classical features of neuronal loss, phospho-TDP-43 inclusions and astrogliosis.

Following cellular transfection, the R235Q mutant formed detergent resistant ubiquitinated cytoplasmic aggregates that sequestered wild-type Annexin A11 and were cytotoxic. The sequestering of wild-type Annexin A11 suggests that Annexin A11 may self-interact. Evidence for this exists from another annexin family member, Annexin A2, that forms hetero-tetramers via bridging with its N-terminal binding partner S100A10 [23]. Calcyclin is known to bind to Annexin A11 and to itself so could form a similar heterotetramer [24]. Although the R235Q mutant failed to bind to calyculin over-expression of calyculin completely cleared insoluble R235Q aggregates by facilitating proteasomal degradation. More subtle differences in calyculin binding were also observed for other Annexin A11 mutants. Calyculin binding was inhibited by D40G and G189E mutations and consistently increased above wild-type for the G38R mutant. Calyculin is known to play a role in proteostasis as it forms a functional complex with calyculin binding protein (CACYPB) and the RING type E3 Ubiquitin Ligase SIAH-1 that regulates ubiquitination and degradation of synaptophysin and binds with alpha-synuclein [25, 26]. Therefore loss of calyculin binding may result in an accumulation of cytoplasmic ANXA11 promoting its aggregation.

We and others have shown that the levels of calyculin are greatly increased in astrocytes in sporadic ALS cases as well as the one carrying the D40G mutation [21, 22]. Even though this phenomenon is not solely linked to Annexin A11 mutations, it raises the possibility that increased astrocytic calyculin expression is a response to defective proteostasis. Interestingly, cells in which TDP43 is knocked-down demonstrate a significant increase in the expression of calyculin transcripts [27]. Additionally, elevated calyculin concentrations can form oligomers that have amyloidogenic properties that have been shown to seed SOD1 aggregation [28].

ANXA11 is a phospholipid binding protein, which may play a role in vesicle trafficking as it has been reported to play a role in apoptosis, exocytosis and cytokinesis [29]. ANXA11 co-localises with calyculin in the nuclear envelope during prophase of mitosis [30], however little is known about its role in post-mitotic neurons. From our study Annexin A11 does form vesicle-like structures in PMNs, which suggests a role for Annexin A11 in vesicular transport. Recent evidence has found that Annexin A11 plays an important structural role in regulating the delivery of vesicular cargoes from the endoplasmic reticulum to the Golgi apparatus which is mediated through its binding to ALG2 to stabilize Sec31A [31]. In our study, Annexin A11 mutations did not directly affect ALG2 binding it is therefore more likely that the mutant alleles disrupt vesicular trafficking by altered binding to calyculin.

We have identified 6 novel, or extremely rare, *ANXA11* mutations in 12 individuals, which account for ~1.2% of familial and 1.7% for sporadic ALS cases. The mutations alter binding to calyculin, which can lead to cytoplasmic aggregation in transfected cells and neuronal cytoplasmic inclusions in a patient carrying the D40G mutation at post mortem. The

identification of *ANXA11* mutations highlights the significance of calcium binding proteins and intracellular trafficking in ALS pathobiology [32]. Further work investigating how mutations affect the folding of annexin A11, its binding to calyculin and the effect on vesicular transport and TDP-43 aggregation will clarify the underlying disease mechanisms.

References

1. Boycott, K.M., et al., *Identification of genes for childhood heritable diseases*. Annu Rev Med, 2014. **65**: p. 19-31.
2. Alonso, A., et al., *Incidence and lifetime risk of motor neuron disease in the United Kingdom: a population-based study*. Eur J Neurol, 2009. **16**(6): p. 745-51.
3. Smith, B.N., et al., *The C9ORF72 expansion mutation is a common cause of ALS+/-FTD in Europe and has a single founder*. Eur J Hum Genet, 2013. **21**(1): p. 102-8.
4. Al-Chalabi, A., et al., *The genetics and neuropathology of amyotrophic lateral sclerosis*. Acta Neuropathol, 2012. **124**(3): p. 339-52.
5. Wu, C.H., et al., *Mutations in the profilin 1 gene cause familial amyotrophic lateral sclerosis*. Nature, 2012. **488**(7412): p. 499-503.
6. Johnson, J.O., et al., *Mutations in the Matrin 3 gene cause familial amyotrophic lateral sclerosis*. Nat Neurosci, 2014. **17**(5): p. 664-6.
7. Bannwarth, S., et al., *A mitochondrial origin for frontotemporal dementia and amyotrophic lateral sclerosis through CHCHD10 involvement*. Brain, 2014. **137**(Pt 8): p. 2329-45.
8. Johnson, J.O., et al., *Exome sequencing reveals VCP mutations as a cause of familial ALS*. Neuron, 2010. **68**(5): p. 857-64.
9. Smith, B.N., et al., *Exome-wide rare variant analysis identifies TUBA4A mutations associated with familial ALS*. Neuron, 2014. **84**(2): p. 324-31.
10. Cirulli, E.T., et al., *Exome sequencing in amyotrophic lateral sclerosis identifies risk genes and pathways*. Science, 2015.
11. Freischmidt, A., et al., *Haploinsufficiency of TBK1 causes familial ALS and fronto-temporal dementia*. Nat Neurosci, 2015.
12. Al-Chalabi, A., et al., *Recessive amyotrophic lateral sclerosis families with the D90A SOD1 mutation share a common founder: evidence for a linked protective factor*. Hum Mol Genet, 1998. **7**(13): p. 2045-50.
13. Nishimura, A.L., A. Al-Chalabi, and M. Zatz, *A common founder for amyotrophic lateral sclerosis type 8 (ALS8) in the Brazilian population*. Hum Genet, 2005. **118**(3-4): p. 499-500.
14. Chio, A., et al., *Large proportion of amyotrophic lateral sclerosis cases in Sardinia due to a single founder mutation of the TARDBP gene*. Arch Neurol, 2011. **68**(5): p. 594-8.
15. Mizutani, A., et al., *The long amino-terminal tail domain of annexin XI is necessary for its nuclear localization*. Arch Biochem Biophys, 1995. **318**(1): p. 157-65.
16. Sudo, T. and H. Hidaka, *Characterization of the calyculin (S100A6) binding site of annexin XI-A by site-directed mutagenesis*. FEBS Lett, 1999. **444**(1): p. 11-4.

17. Drozdetskiy, A., et al., *JPred4: a protein secondary structure prediction server*. Nucleic Acids Res, 2015.
18. Gerke, V., C.E. Creutz, and S.E. Moss, *Annexins: linking Ca²⁺ signalling to membrane dynamics*. Nat Rev Mol Cell Biol, 2005. **6**(6): p. 449-61.
19. Rosengarth, A. and H. Luecke, *A calcium-driven conformational switch of the N-terminal and core domains of annexin A1*. J Mol Biol, 2003. **326**(5): p. 1317-25.
20. Osako, Y., et al., *Autolytic activity of human calpain 7 is enhanced by ESCRT-III-related protein IST1 through MIT-MIM interaction*. FEBS J, 2010. **277**(21): p. 4412-26.
21. Hoyaux, D., et al., *S100A6 overexpression within astrocytes associated with impaired axons from both ALS mouse model and human patients*. J Neuropathol Exp Neurol, 2002. **61**(8): p. 736-44.
22. Hoyaux, D., et al., *S100A6, a calcium- and zinc-binding protein, is overexpressed in SOD1 mutant mice, a model for amyotrophic lateral sclerosis*. Biochim Biophys Acta, 2000. **1498**(2-3): p. 264-72.
23. Ayala-Sanmartin, J., et al., *Insight into the location and dynamics of the annexin A2 N-terminal domain during Ca(2+)-induced membrane bridging*. Biochim Biophys Acta, 2008. **1778**(2): p. 472-82.
24. Lesniak, W., L.P. Slomnicki, and A. Filipek, *S100A6 - new facts and features*. Biochem Biophys Res Commun, 2009. **390**(4): p. 1087-92.
25. Wheeler, T.C., et al., *Regulation of synaptophysin degradation by mammalian homologues of seven in absentia*. J Biol Chem, 2002. **277**(12): p. 10273-82.
26. Lee, J.T., et al., *Ubiquitination of alpha-synuclein by Siah-1 promotes alpha-synuclein aggregation and apoptotic cell death*. Hum Mol Genet, 2008. **17**(6): p. 906-17.
27. Polymenidou, M., et al., *Long pre-mRNA depletion and RNA missplicing contribute to neuronal vulnerability from loss of TDP-43*. Nat Neurosci, 2011. **14**(4): p. 459-68.
28. Botelho, H.M., et al., *S100A6 amyloid fibril formation is calcium-modulated and enhances superoxide dismutase-1 (SOD1) aggregation*. J Biol Chem, 2012. **287**(50): p. 42233-42.
29. Wang, J., et al., *Annexin A11 in disease*. Clin Chim Acta, 2014. **431**: p. 164-8.
30. Tomas, A., C. Futter, and S.E. Moss, *Annexin 11 is required for midbody formation and completion of the terminal phase of cytokinesis*. J Cell Biol, 2004. **165**(6): p. 813-22.
31. Shibata, H., et al., *A new role for annexin A11 in the early secretory pathway via stabilizing Sec31A protein at the endoplasmic reticulum exit sites (ERES)*. J Biol Chem, 2015. **290**(8): p. 4981-93.
32. Leal, S.S. and C.M. Gomes, *Calcium dysregulation links ALS defective proteins and motor neuron selective vulnerability*. Front Cell Neurosci, 2015. **9**: p. 225.
33. Maekawa, S., et al., *TDP-43 is consistently co-localized with ubiquitinated inclusions in sporadic and Guam amyotrophic lateral sclerosis but not in familial amyotrophic lateral sclerosis with and without SOD1 mutations*. Neuropathology, 2009. **29**(6): p. 672-83.

Acknowledgements and Funding

Funding for this work was provided by The Middlemass family, Heaton-Ellis Trust, Motor Neurone Disease Association, Medical Research Council, The Psychiatry Research Trust of the Institute of Psychiatry, Guy's and St Thomas' Charity, the Wellcome Trust and the Noreen Murray Foundation. This is an EU Joint Programme - Neurodegenerative Disease Research (JPND) project. The project is supported through the following funding organisations under the aegis of JPND - www.jpnd.eu (United Kingdom, Medical Research Council and Economic and Social Research Council). CES and AAC receive salary support from the National Institute for Health Research (NIHR) Dementia Biomedical Research Unit at South London and Maudsley NHS Foundation Trust and King's College London. CF received salary support from ALSA. The views expressed are those of the authors and not necessarily those of the NHS, the NIHR or the Department of Health. The work leading up to this publication was funded by the European Community's Health Seventh Framework Programme (FP7/2007–2013; grant agreement number 259867). Samples used in this research were in part obtained from the UK National DNA Bank for MND Research, funded by the MND Association and the Wellcome Trust. We would like to thank people with MND and their families for their participation in this project. We acknowledge sample management undertaken by Biobanking Solutions funded by the Medical Research Council at the Centre for Integrated Genomic Medical Research, University of Manchester.

Conflicts of Interest

None.

Author Contributions

B.N.S, S.T, C.F, H.S, H.C, C.T, A.K, S.A.S, J.L, V.S and C.E.S designed the experiments. B.N.S, S.T, C.F, H.S, H.C, C.T, A.K N.T, K.K, C.V, A.S, A.S.G, J.M, C.H.W, M.M, W.K, P.S, N.P and M.N performed the experimental procedures and analyzed the data. P.N, F.B, V.J, A.A, A.R, J.B, J.P, C.T, F.V, S.D, N.L, H.P, K.M, A.A.C, P.J, J.K, M.T, K.T, O.H, J.G, J.D.B, C.G, A.R, R.B, S.A.S, V.S, J.L and C.E.S collected and/or contributed DNA samples or exome sequences. B.N.S and C.E.S wrote the manuscript with contributions from the authors.

Supplementary Materials and Methods

DNA Samples

Full patient consent was provided by FALS index patients and control individuals for research purposes. All patients had a diagnosis of definite or probable ALS based on revised El Escorial criteria (Brooks, 2000) with at least one relative known to have ALS+/-FTD. All FALS were pre-screened for known causative ALS genes and individuals carrying mutations in *SOD1*, *C9ORF72* (GGGGCC expansion), *TARDBP*, *FUS*, *PFN1*, *UBQLN2*, *MATR3*, *CHCHD10*, *TBK1*, *OPTN*, *VAPB* and *VCP* were excluded from the study. The discovery cohort was comprised of 403 FALS sourced from the UK (163), Italy (97), the United States (90), Spain (30), Ireland (17), Belgium (3) and the Netherlands (3). An additional 58 subjects were exome captured where the primary causative mutation had previously been determined (*FUS*, *TARDBP* or *SOD1*). Furthermore, DNA of at least one affected family member was available from 27 index cases and was exome sequenced in tandem for segregation analysis.

The replication cohort consisted of a total of 204 cases pre-screened for known ALS genes (above) from the United States (132), Italy (25), the UK (20), Germany (20), and Canada (7). An additional 47 subjects were exome captured where the likely pathogenic mutation has already been determined, plus the affected relatives of 28 of the index cases in the replication cohort. Sequence data for 109 cases in the replication cohort were obtained, with permission, from the dbGAP repository (NIH Exome Sequencing of Familial Amyotrophic Lateral Sclerosis, NINDS, phs000101.v4.p1, Traynor)

Exome Sequencing and Bio-informatic Analysis

Exome sequencing paired-end FASTQ files were aligned to the hg19 human reference using NovoCraft Novoalign, and variants called with samtools v1.1 mpileup. VCF files were filtered at DP \geq 10 and GQ \geq 20, and normalized with bcftools v1.1 norm. Functional annotation and matches to 1000genomes and 672 local control exomes were added with table_annoar.pl (Wang K, Li M, Hakonarson H. [ANNOVAR: Functional annotation of genetic variants from next-generation sequencing data](#) *Nucleic Acids Research*, 38:e164, 2010). Matches to other public variant resources (ExAC, ESP, UK10K, dbSNP142) were added via custom perl scripts. Effects on splicing were assessed using Netgene2 (Brunak, S., Engelbrecht, J., and Knudsen, S., Prediction of Human mRNA Donor and Acceptor Sites from the DNA Sequence. *Journal of Molecular Biology*, 1991, 220, 49-65.) but no significant changes found between the wild type or any ANXA11 variant sequence.

All novel variants (defined as absent from ExAC (<http://exac.broadinstitute.org/>), ESP (<http://evs.gs.washington.edu/EVS/>), UK10K (<http://www.uk10k.org/>) and 772 In-house exome controls) shared between unrelated index cases where at least one sample had a GQ $<$ 90 were manually inspected using a combination of the Integrative Genomics Viewer and UCSC Blat, and without exception rejected due to either misalignment of reads from close paralogues or local alignment error adjacent to common indels. It is possible that some of the remaining variants found in two samples are also false positives, but those variants shared by three or more cases have all been verified by this method.

Genetics Screening

All coding exons of *ANXA11* (Refseq ID NM_145869) were amplified using standard polymerase chain reaction procedures. At least 100bp of flanking intronic sequence was included to detect splice site mutations. Amplicons were directly sequenced with Big-Dye Terminator v1.1 on an ABI3130 genetic analyzer (Applied Biosystems Pty Ltd, Warrington, UK) and sequence chromatograms analyzed for mutations using Sequencher 4.10 directly by eye (Gene Codes Corporation, Ann Arbor, Michigan, USA). Reconfirmation of novel mutations was conducted by re-dilution of stock DNA and re-PCR and direct sequencing. Rare variant positions in *ANXA11* were also filtered against 3596 Italian exome controls. Nine hundred and nine local control UK samples matched for sex and age were assayed for *ANXA11* genomic SNP positions for the G38R, D40G, G189E and R235Q mutations using KASPar genotyping methods by LGC Genomics (LGC Genomics, Teddington, UK).

Plasmids and Cloning

A cDNA encoding ANXA11 was amplified from pEGFP-C3/ANXA11 (Tomas and Moss, 2003) with the following pair of oligonucleotides with a *Bam*HI site (underlined): 5'-TAGGATCCACCATGAGCTACCCTGGCTATCC-3' (sense) and 5'-GCGGATCCGAGTCATTGCCACACAGATCTT-3' (antisense). The DNA fragment obtained was subcloned

into the pCR-BluntII-TOPO (Invitrogen). To construct pANXA11-SGFP2, a *Bam*HI fragment from pCR-Blunt II-TOPO/ANXA11 was inserted into the *Bam*HI site of pSGFP2-N-SGG (Shibata et al. 2010). Single amino acid changes (G38R, D40G and R235Q) were introduced into pANXA11-SGFP2 by PCR-based site-directed mutagenesis. To construct pFLAG-S100A6, an *Eco*RI fragment of pCR2.1 TOPO/S100A6 (kindly provided by Dr. Kiyotaka Hitomi, Nagoya University, Japan) was inserted into the *Eco*RI site of pCMV3xFLAG-B (Kato et al. 2003). A cDNA encoding sorcin was amplified from human fetus cDNA library (Clontech) and subcloned into the pCMV-Tag 2A (Stratagene) to construct pFLAG-sorcin. An expression vector encoding ALG-2 N-terminally tagged with FLAG (pFLAG-ALG-2 RNAi^R) was described previously (Okumura et al. 2009).

ANXA11 expression vectors (Gateway pcDNA3.1/nV5-DEST, Invitrogen) encoding c-terminal HA tagged ANXA1 wild type (WT), G38R, D40G and R235Q mutants were used in this study. Site-directed mutagenesis was performed according to the manufacturer's protocol (Quickchange II Site-Directed Mutagenesis Kit, Stratagene) using a ANXA11-HA tagged pDONR221 entry clone plasmid to produce constructs harboring the novel mutants identified in this study. The pDONR221-ANXA11 mutant constructs were then recombined with pcDNA3.1/nV5-DEST to create the final mutant expression constructs. All constructs were verified by sequencing.

Antibodies

Mouse monoclonal anti-GFP at 1/2000 (cat.no sc-9996, Santa Cruz, Dallas, USA), mouse monoclonal anti-GAPDH (cat.no G8795, Gillingham, UK) and mouse monoclonal Histone H3 (cat.no 96C10, New England Biolabs Hitchin, UK) were used for detecting lysate, soluble and insoluble fractions on Western blot from NP40 insolubility assays. Mouse monoclonal anti-GFP at 1/2000 (cat.no sc-9996), FLAG-M2 (mouse) was used to detect FLAG-ALG2 and FLAG-Sorcin and rabbit FLAG (cat.no. F7425, Sigma) were using in the Annexin A11:calcylin binding assays. Polyclonal Rabbit Anti-ANXA11 (cat.no. 10479-2-AP, Proteintech, Manchester, UK) was used for ANXA11^{R235Q} staining of HEK cells (Supplementary Figure 2) and spinal cord of the D40G SALS patient, SALS patient devoid of known ALS causing mutation and controls. Polyclonal rabbit Anti-calcylin (cat.no. 10245-1-AP, Proteintech) was utilized for IHC of patient and control post mortem tissue.

Transfection of HEK293T Cells

HEK293T cells were maintained in DMEM with high glucose plus Glutamax (Life Technologies, Paisley, UK) with 10% fetal bovine serum, 100 U/mL penicillin, and 100 mg/mL streptomycin in a water jacketed incubator at 5% CO₂. For solubility fractionation, transfections were performed in 12-well plates with 500 ng of plasmid DNA and 1.5 mL of Fugene HD (Promega, Southampton, UK) per well, as per the manufacturer's protocol. For immunofluorescence, HEK293T cells were plated at 25,000 cells/cm² on 13 mm diameter, 1.5-mm-thickness coverslips coated with poly-D-lysine (Sigma-Aldrich, Dorset, UK) in 24-well plates and transfected with 250 ng of DNA and 0.75 mL of Fugene HD.

Cell Survival GFP FACS Analysis

For cell survival assay, SH-SY5Y cells were trypsinised and stained with Calcein Violet 450AM Viability Dye (500 nM, eBioscience) for 30 min at room temperature. After washed twice with PBS, cells were resuspended in PBS and analysed with BD FACS Cantoll (BD Biosciences).

FLAG-S100A6 and ANXA11-GFP Binding Assays

HEK293 YS14 cells (a sub-cloned HEK293 cell line) (Shibata et al. 2007) which had been plated on the previous day at a density of 2×10^6 cells per 10 cm dish were transfected with expression plasmids using Polyethyleneimine (150 µg) (Polysciences) and then cultured for 24 hr. To attain equivalent expression level, the following amounts of plasmid DNA for SGFP2-fused proteins were used: pSGFP2-N-SGG, 3 µg; pANXA11^{WT}-SGFP2, 5 µg; G38R, 6 µg; D40G, 7 µg; G189E, 6 µg; R235Q, 10 µg. The cells were washed and harvested with PBS, suspended in 470 µL per 10 cm dish (for cells expressing SGFP2-fused proteins) or in 350 µL per 10 cm dish (for cells expressing FLAG-tagged proteins) of lysis buffer (20 mM HEPES-KOH, pH 7.2, 142.5 mM KCl, 2.5 mM MgCl₂) containing 0.2% Triton X-100, 10 µM EGTA, protease inhibitors (1 µM E64, 3 µg/mL leupeptin, 0.1 mM pepabloc, 2 µM pepstatin A, 0.2 mM PMSF) and phosphatase inhibitors (50 mM NaF, 10 mM β-glycerophosphate, 1 mM Na₃VO₄). After 30 min on ice, the cell lysates were centrifuged at 15,000 g for 10 min at 4°C. The cleared lysates of the cell expressing SGFP2-fused proteins were divided into aliquots of 200 µL and mixed with 100 µL of the cleared lysates of the cells expressing FLAG-tagged proteins. Twenty µL of the mixture was

taken as input. The samples were rotated at 4°C for 90 min in the presence of 100 µM of CaCl₂, mixed with 0.8 µg of mouse antibody against FLAG (M2) and rotated at 4°C for further 60 min. Then the samples were incubated overnight at 4°C with 10 µL of Dynabeads Protein G (Novex, Invitrogen). The beads were collected using a magnet and washed twice with 500 µL of lysis buffer containing 0.1% Triton X-100 and 100 µM CaCl₂. Washed beads were boiled for 5 min in 56 µL of 1x SDS-PAGE sample buffer. Four µL of input and 8 µL of IP (for detection of FLAG-tagged proteins) or 1.2 µL of input and 12 µL of IP (for detection of SGFP2-fused proteins) were run on a western blot.

FLAG-Calcyclin and ANXA11-GFP over-expression in HEK cells

500ng of ANXA11-GFP^{WT} and ANXA11-GFP^{R235Q} constructs were co-transfected with 500ng of FLAG-Calcyclin in a 6 well dish of HEK cells plated at 25,000 cells/cm². Untreated ANXA11-GFP^{WT} and ANXA11-GFP^{R235Q} were co-transfected with empty pEGFP-C1 vector (Clontech Pty Ltd, Mountain View, California, USA). Duplicate wells of ANXA11-GFP^{WT} and ANXA11-GFP^{R235Q} transfected cells were also treated with 0.5µM MG132 24hrs before harvesting (48 hours post transfection). Cells were harvested and processed as per the NP40 insolubility assay listed below.

Primary Motor Neuron (PMN) Cultures

Motor neurons were isolated from mouse embryos, cultured and transfected as described (Fallini et al, Mol. Neurodegen., 2010). Cells were fixed 1 or 4 days after transfection and processed for immunofluorescence. After antigen retrieval in citrate buffer for 20 minutes and blocking in 5% bovine serum albumin for 1 hour, cells were hybridized overnight at 4°C with HA primary antibody (Covance, 1:1000) Alexa488 or Alexa594-conjugated secondary antibodies (Jackson Immunoresearch) were incubated for 1 hour at room temperature.

Protein Fractionation and Insolubility Assay

ANXA11-GFP WT and mutant construct transfected HEK cells were harvested at 48 wells post-transfection and fractionated using a NP40 solubility assay as described previously (Smith et.al Neurobiology of Aging 2015). Lysate and soluble fractions were quantified using a BSA standard protein assay and 5ug of lysate and soluble fractions analysed by Western blotting. The same volume of insoluble fraction was loaded as per cell lysate. Nitrocellulose membranes were probed with mouse monoclonal anti-GFP at 1/2000 dilution, mouse monoclonal ant-GAPDH 1/2000 dilution and mouse monoclonal Histone H3 1/1000 dilution in 1% Skim Milk and PBS-Tween. Band intensities were quantified using Image J (<http://imagej.nih.gov/ij/>).

Statistical Analysis

Statistical analysis of PMN immunofluorescence data and NP40 insolubility data was performed with Graphpad Prism software. Normality of the datasets was assessed with the D'Agostino-Pearson test. One-way ANOVA with Dunnett's post *hoc* test or Kruskal-Wallis with Dunn's post *hoc* test were performed depending on normality.

Mutation modelling and Jpred Analysis

The Refseq protein database was searched with human ANXA11 (NP_001148.1) via BlastP at the NCBI (<http://blast.ncbi.nlm.nih.gov/Blast.cgi>). The highest matching sequence per vertebrate species from the first 250 results was aligned with all others using Muscle (<http://www.ebi.ac.uk/Tools/msa/muscle/>). Sequences were removed if they had a better reciprocal match to a different human annexin gene or if they contained significant numbers of gaps, mismatching regions or consecutive "X"s, implying incomplete or mistranslated sequence. Fish were also excluded, as they consistently showed significant divergence along the majority of the N-terminus, and with the exception of the first 20 amino acids a satisfactory alignment to other Classes could not be obtained. The resulting multiple alignment was hand edited in GeneDoc and submitted to JPred4 (<http://www.compbio.dundee.ac.uk/jpred4/>) for secondary structure prediction. Predictions were also made for the ALS-associated variants G38R and D40G, and the non-ALS D40H negative-control variant (rs368751524, found once in the ExAC dataset) by replacing every amino acid in the multiple alignment with the variant residue. Possible amphipathicity of any resulting alpha helices was tested by submitting the sequences to Helixator (http://www.tcdb.org/progs/helical_wheel.php). The procedure was then repeated for human ANXA1, but with this gene it was not necessary to exclude fish from the alignment.

Neuropathology

Brain tissue samples in 10% formalin-fixed, paraffin-embedded tissue blocks were available from the London Neurodegenerative Diseases Brain Bank (King's College London, UK). Consent for autopsy, neuropathological assessment and research were obtained from all subjects and all studies were carried out under the ethical approval of the tissue bank. Block taking for histological and immunohistochemical studies and neuropathological assessment for neurodegenerative diseases was performed in accordance with standard criteria.

Immunohistochemistry:

Immunohistochemistry was carried out as per previously published protocols [33]. In brief, sections of 7µm thickness were cut from the paraffin-embedded tissue blocks, deparaffinised in xylene, endogenous peroxidase was blocked by 2.5% H₂O₂ in methanol and immunohistochemistry performed. To enhance antigen retrieval, sections were kept in citrate buffer for 10 minutes following microwave treatment. After blocking in normal serum primary antibody was applied overnight at 4°C. Following washes, sections were incubated with biotinylated secondary antibody (DAKO), followed by avidin:biotinylated enzyme complex (Vectastain Elite ABC kit, Vector Laboratories, Peterborough, UK). Finally sections were incubated for 10–15 min with 0.5 mg/mL 3,3'-diaminobenzidine chromogen (Sigma-Aldrich Company Ltd, Dorset UK) in Tris-buffered saline (pH 7.6) containing 0.05% H₂O₂. Sections were counterstained with Harris' haematoxylin and immunostaining analysed using a Leica microscope (Leica, Wetzlar, Germany).

Double Immunofluorescence:

7µm sections were cut from formalin fixed paraffin embedded blocks, dewaxed in xylene and dehydrated in 99% industrial methylated spirit. Sections were then pretreated by microwaving in citrate buffer and blocked using normal goat serum (1:10 for 45min). Primary antibodies were then applied and sections incubated at 4°C overnight. Sections were washed and secondary Alexa Fluor antibody (Invitrogen, Paisley, UK) applied for 45 min (in dark). Autofluorescence was quenched by incubating the sections in Sudan black for 10min followed by numerous washes in phosphate buffered saline before coverslip mounting using hard set media with DAPI. Sections were visualised using a fluorescent microscope (Zeiss Axiovert S 100, Gottingen, Germany) and images captured using ImagePro Express (V6).

References

- Fallini C, Bassell GJ, Rossoll W (2010) High-efficiency transfection of cultured primary motor neurons to study protein localization, trafficking, and function. *Mol Neurodegener.* 2010 Apr 21;5:17.
- Katoh, K., Shibata, H., Suzuki, H., Nara, A., Ishidoh, K., Kominami, E., Yoshimori, T., and Maki, M. (2003) The ALG-2-interacting protein Alix associates with CHMP4b, a human homologue of yeast Snf7 that is involved in multivesicular body sorting. *J Biol Chem.* 278, 39104-39113
- Maekawa S, Leigh PN, King A, Jones E, Steele JC, Bodi I, Shaw CE, Hortobagyi T, Al-Sarraj S (2009). TDP-43 is consistently co-localized with ubiquitinated inclusions in sporadic and Guam amyotrophic lateral sclerosis but not in familial amyotrophic lateral sclerosis with and without SOD1 mutations. *Neuropathology.* 2009 Dec;29(6):672-83.
- Okumura, M., Ichioka, F., Kobayashi, R., Suzuki, H., Yoshida, H., Shibata, H., and Maki, M. (2009) Penta-EF-hand protein ALG-2 functions as a Ca²⁺-dependent adaptor that bridges Alix and TSG101. *Biochem. Biophys. Res. Commun.* 386, 237-241
- Shibata, H., Suzuki, H., Yoshida, H., and Maki, M. (2007) ALG-2 directly binds Sec31A and localizes at endoplasmic reticulum exit sites in a Ca²⁺-dependent manner. *Biochem. Biophys. Res. Commun.* 353, 756-763
- Shibata, H., Inuzuka, T., Yoshida, H., Sugiura, H., Wada, I., and Maki, M. (2010) The ALG-2 binding site in Sec31A influences the retention kinetics of Sec31A at the endoplasmic reticulum exit sites as revealed by live-cell time-lapse imaging. *Biosci. Biotechnol. Biochem.* 74, 1819-1826
- Smith B, Ticozzi N, Fallini C et.al (2014). Exome-wide rare variant analysis identifies TUBA4A mutations associated with familial ALS. *Neuron.* 2014 Oct 22;84(2):324-31.
- Tomas, A., and Moss, S. E. (2003) Calcium- and cell cycle-dependent association of annexin 11 with the nuclear envelope. *J. Biol. Chem.* 278, 20210-20216

Figure Legends

Main Figures

Figure 1. Annexin A11 mutations identified in ALS patients following stringent filtering of exome sequencing data. (A and B) Pedigrees of Family 1 and 2 respectively, carrying the p.D40G mutation. Family members for whom DNA was available for segregation analysis are labelled with M/W for a heterozygous mutant (A>G allele) or W/W for a homozygous reference allele. The gender has been anonymised for each individual. Affected individuals with ALS are denoted by a solid black diamond, unaffected by white diamonds and unaffected carriers with a black dot. . Index cases exome sequenced as part of this study are marked with a blue star. (C) The G175R mutation segregates in both an index case and affected sibling. (D) Schematic representation of the Annexin A11 molecule highlighting a clustering of mutations in the N-terminus (first 196 residues). Mutation positions in the N-terminus are fully conserved in mammals, and conserved in birds, amphibians and reptiles if in an annexin domain. Mutations identified in the discovery cohort are red, replication cohort blue and those found in sporadic ALS cases yellow. The binding site of calyculin (labelled CACY) is located in the N-terminus, residues 50-62.

Figure 2. TDP-43 and Annexin A11 immunohistochemistry from post-mortem spinal cord tissue of a SALS cases harbouring the novel D40G mutation. (A) phospho-TDP43 positive cytoplasmic inclusion from anterior horn of the spinal cord. (B-E) Annexin A11 positive inclusions in motor neurons of the cord included skein like (B), filamentous and tubular-shaped structures (C-D). Occasional more “basket-like” inclusions were seen in the cord (E). (F) Abundant annexin A11 positive torpedo-like neuritic structures were also present in the neuropil here seen in the motor cortex. (arrows) (G-H) Representative spinal cord staining in a SALS case (n=4) negative for *Annexin A11* mutations and known ALS mutations and a control individual (n=4). (I-J) Double labelling for phospho-TDP43 (green) and Annexin A11 aggregates (red). (K-L) Co-staining for ubiquitinated aggregates (red= Annexin A11 and green=ubiquitin) showed occasional co-localisation (indicated by arrows). Scale bars - A,E,G and H- 30µm; B, C- 20µm; D-15µm; F 50µm, I,J- 25µm, K,L- 50µm.

Figure 3. Functional Annexin A11 studies in mouse Primary Motor Neurones and SH-SH5Y cells. (A) ANXA11-HA^{WT/G38R/D40G/R235Q} transfected into PMNs display cytoplasmic vesicle-like structures for WT, G38R and D40G and a significant localization of smaller cytoplasmic foci in the cytoplasm, (B) p=0.0004 (One way ANOVA and Dunnett's post hoc test, Bars represent mean and SEM). Vesicles were defined as structures with a diameter between 0.5µm to 1.9 µm (mean 1 µm) and foci 0.16µm to 0.5 µm (mean 0.3 µm). (C) There was a significant proportion of foci associated with R235Q (p<0.0001, One way ANOVA and Dunnett's post hoc test) but a smaller proportion of vesicle like structures associated with G38R and a complete absence with R235Q (p=0.0051 and p<0.0001 respectively, One way ANOVA and Dunnett's post hoc test). (D) Co-expression of ANXA11-HA^{WT} and ANXA11-GFP^{R235Q} in SH-SH5Y cells demonstrated co-localisation suggesting sequestering of ANXA11-HA^{WT} by mutant ANXA11, possibly acting in a dominant negative manner. (E) Co-expression of ANXA11-HA^{WT/G38R/D40G/R235Q} with the C-terminal fragment of TDP-43-GFP (residues 208-414), showing a significant co-localization of R235Q with TDP43 (p=0.0003, One way ANOVA and Dunnett's post hoc test) and a significant engulfment of D40G by TDP43 (p=0.001 One way ANOVA and Dunnett's post hoc test). Scalebars (A,D and E) 10µm.

Figure 4. Calcyclin analysis: *in-vitro* binding assays with mutant Annexin A11 constructs and staining of post-mortem tissue. (A) Representational western blot demonstrating lack of binding of FLAG-calcyclin to ANXA11-GFP^{D40G}, ANXA11-GFP^{G189E} and ANXA11-GFP^{R235Q} by immunoprecipitation (n=3). The top panel shows GFP intensities of input and pulled down fractions, with IgG heavy (50kDa) and light (25kDa) chains indicated. The bottom panel illustrates input and IP levels of FLAG-calcyclin. (B) Cross-section of spinal cord showing calcyclin expression in (i) control and (ii) SALS case with the p.D40G mutation. High calcyclin expression can be seen in the lateral corticospinal tracts (arrows). High magnification revealed glial and neuropil staining in the lateral corticospinal tract (data not shown). (iii) SALS case devoid of known ALS causing mutation but also displaying strong expression of calcyclin in the lateral corticospinal tracts (arrows). Scale bars (i) 40µm, (ii) 30µm and (iii) 25µm (C) NP40 insolubility assay of co-expression of 500ng of ANXA11-GFP^{WT} and ANXA11-GFP^{R235Q} and 500ng of FLAG-calcyclin (labelled C in image) in HEK cells, demonstrating clearance of insoluble R235Q aggregates by calcyclin co-expression. An equivalent amount of empty GFP Vector (500ng) was added to untreated WT and R235Q HEK cells. (D) Quantification of ANXA11-GFP^{WT and R235Q} co-expression experiment. Bands were quantified with ImageJ (<http://imagej.nih.gov/ij/>) and intensity levels were calculated with respect to untreated ANXA11-GFP^{WT} and a one-way ANOVA test demonstrating significance of the R235Q untreated and R235Q treatment with calcyclin and MG132 treatment for 24hours (p<0.01 and p<0.001 respectively).

Supplementary Figures

Supplementary Figure 1. The *Annexin A11* p.D40G mutation shares a common haplotype comprised of 8 SNPs and 2 microsatellites. Micro 1 and Micro 2 are two uncharacterised tri and di nucleotide repeat sequences identified from the hg19 reference genome (genome.ucsc.edu). Shaded yellow region denotes the region containing the *Annexin A11* gene. The common conserved haplotype in members with the D40G mutation is indicated by a grey bar. Individuals with Annexin A11 mutations are labeled according to Supplementary Table 3.

Supplementary Figure 2. R235Q ANXA11-GFP co-localises with ubiquitin and p62 in HEK cells. Cells were transfected with ANXA11-GFP^{R235Q} for 48hrs, fixed and stained with the following antibodies (A) mouse GFP green. (B) ANXA11 Polyclonal rabbit Antibody (Proteintech) red. (C) Merge of A, B and DAPI blue nuclear staining, showing specificity of ANXA11 specific antibody. , (D) mouse GFP green. (E) Rabbit K-48 Ubiquitin red. (F) Merge of D, E and DAPI. (G) mGFP green. (H) Rabbit p62 red. (I) Merge of G, H and DAPI.

Supplementary Figure 3. R235Q ANXA11-GFP forms high molecular weight detergent resistant aggregates in HEK cells. (A) The lysate (L), soluble (S) and insoluble (I) fractions of HEK cells transfected with ANXA11-GFP^{WT/G38R/D40G/G189E/R235Q} shows R235Q to form high detergent resistant insoluble aggregates. (B) The level of R235Q insoluble fraction is statistically significant when compared with WT (p=0.007, One way ANOVA with Dunnett's post hoc test).

Supplementary Figure 4. Cell survival assay of ANXA11-GFP WT and mutant constructs shows R235Q to be toxic in SH-SH5Y cells. SH-SH5Y cells transfected with ANXA11-GFP empty vector, WT and mutant constructs were harvested at 48hrs post transfection and the percentage of GFP positive apoptotic cells determined by FACS analysis. (n=3). ANXA11-R235Q was the only mutant to be statistically significant compared to WT (p=0.0001, one way ANOVA with Dunnett's post hoc test).

Supplementary Figure 5. Modelling of Annexin A11 identifies two amphipathic helices in the N-terminus of Annexin A11 that overlap the G38 and D40 residues. (A) Jpred secondary structure prediction focusing on the N-terminus (residues 1-270) using a multiple alignment of all mammalian orthologue sequences identified two amphipathic helices, indicated in red (residues 38-45 and 50-60). Known annexin domains start at ~200 residues. The locations of the G38 and D40 residues are indicated in the first amphipathic helix. (B) Protein structure of Annexin A1 (pdb:1hm6) in the presence of calcium, with the annexin domain alpha helices in red and the N-terminal helices in magenta. (C) Jpred also predicts the N-terminus of Annexin A1 to possess two amphipathic helices (residues 2-14 and 19-26). (D) Jpred predicts the G38R variant to change the first amphipathic helix to a beta-sheet whilst the D40G variant also severely disrupts it.

Supplementary Figure 6. N-terminal Annexin A11 mutations do not alter binding of Sorcin and ALG2. (A) Immunoprecipitation (IP) of FLAG-Sorcin from mixed lysates of HEK cells transfected with ANXA11-GFP^{WT+G38R+D40G+G189E+R235Q} activated with calcium show no difference in binding between ANXA11 WT and mutants when probed for GFP. (B) The same was seen when IP was conducted with ALG2-sorcin. (n=3). The top panel shows GFP intensities of input and pulldown fractions, with IgG heavy and light chains indicated. The bottom panel for both (A) and (B) illustrates input and IP levels of FLAG-sorcin or FLAG-ALG2 respectively.

Supplementary Tables

Supplementary Table 1. Analysis of FALS exomes identifies 12 known ALS mutations and 95 novel variants shared by two or more index cases. Twelve previously identified disease causing mutations (all from *SOD1*, *FUS* or *TARDBP*, shaded in grey) were identified in two or more of 713 FALS index cases, after stringent quality filtering and exclusion of variants found in >60,000 control exomes. When the 105 samples with a known ALS mutation were removed, there were 95 novel variants shared by two or more of the remaining 608 FALS cases.

Supplementary Table 2. All ANXA11 variants identified in in discovery and replication FALS cohorts and UK SALS cases. The ATG of *ANXA11* cDNA is defined as +1 according to HGVS guidelines (<http://www.hgvs.org/>), Refseq NM_145869. A high depth (mean of 63.3 reads) and degree of coverage (>10X in over 91% of samples) was observed in exome sequencing reads across the *ANXA11* coding region. Frequencies for each variant were assessed in dbSNP132, ESP, ExAC, 1000 Genomes, UK10K, and also 672 non-neurological Kings College London (KCL) exomes. An additional 909 and 3596 UK local and Italian exome controls respectively were used to further assess frequencies for the p.G38R, D40G, P108L, G175R, G189E, R235Q and R346C variants. Polyphen predicts most *ANXA11* novel mutations to be damaging. * Also harbored a *C9ORF72* expansion. # Did not segregate in other affected family members, therefore are considered benign private polymorphisms. na – not applicable.

Supplementary Table 3. Clinical details of patients with ANXA11 mutations. Most patients with N-terminal mutations have late disease onset (average of 72years). Patients carrying a D40G mutation have predominantly bulbar onset. There was a distinct absence of FTD symptoms in all *ANXA11* carriers.

Supplementary Table 1. 95 Single nucleotide variants present in 2 or more FALS but absent in all control databases

Chr	Start (hg19)	End (hg19)	Gene Status	Gene	AA Change	cdna change	Exon	LongRef_Details	FALS_index_hets	Discovery	Replication
21	33039672	33039672	Known	SOD1	I114T	341T>C	exon4	154:NP_000445:NM_000454	10	9	1
1	11082610	11082610	Known	TARDBP	A382T	1144G>A	exon6	414:NP_031401:NM_007375	6	1	5
21	33032096	33032096	Known	SOD1	A5V	14C>T	exon1	154:NP_000445:NM_000454	5	3	2
16	31202739	31202739	Known	FUS	R521C	1561C>T	exon15	526:NP_004951:NM_004960	4	3	1
1	11082475	11082475	Known	TARDBP	M337V	1009A>G	exon6	414:NP_031401:NM_007375	3	3	0
16	31202752	31202752	Known	FUS	P525L	1574C>T	exon15	526:NP_004951:NM_004960	3	2	1
21	33039612	33039612	Known	SOD1	G94D	281G>A	exon4	154:NP_000445:NM_000454	3	1	2
1	11082536	11082536	Known	TARDBP	G357D	1070G>A	exon6	414:NP_031401:NM_007375	2	2	0
16	31202282	31202282	Known	FUS		1394-2A>-	exon14	526:NP_004951:NM_004960	2	1	1
21	33040861	33040861	Known	SOD1	L145F	435G>C	exon5	154:NP_000445:NM_000454	2	1	1
1	11082501	11082501	Known	TARDBP	N345K	1035C>A	exon6	414:NP_031401:NM_007375	2	0	2
21	33039677	33039677	Known	SOD1	R116G	346C>G	exon4	154:NP_000445:NM_000454	2	0	2
21	28212087	28212087	Novel	ADAMTS1		1853-6T>A	exon8	967:NP_008919:NM_006988	2	1	1
14	78325590	78325590	Novel	ADCK1	R131C	391C>T	exon4	523:NP_065154:NM_020421	2	2	0
14	96944819	96944819	Novel	AK7	D525H	1573G>C	exon15	723:NP_689540:NM_152327	2	1	1
9	116151928	116151928	Novel	ALAD	R222H	665G>A	exon9	330:NP_000022:NM_000031	2	1	1
10	81930608	81930608	Novel	ANXA11	D40G	119A>G	exon5	505:NP_665876:NM_145869	3	2	1
10	99016185	99016185	Novel	ARHGAP19		841-24T>G	exon7	494:NP_116289:NM_032900	2	2	0
3	35833976	35833976	Novel	ARPP21	P713L	2138C>T	exon18	813:NP_001254548:NM_001267619	3	2	1
19	57746688	57746688	Novel	AURKC	P278L	833C>T	exon7	309:NP_001015878:NM_001015878	2	1	1
9	136910498	136910498	Novel	BRD3	A378T	1132G>A	exon7	726:NP_031397:NM_007371	2	1	1
9	116132106	116132106	Novel	BSPRY	Y298C	893A>G	exon6	402:NP_060158:NM_017688	2	2	0
6	41898380	41898380	Novel	BYSL	S193F	578C>T	exon4	437:NP_004044:NM_004053	2	0	2
7	143002126	143002126	Novel	CASP2	R441S	1321C>A	exon11	452:NP_116764:NM_032982	2	0	2
10	33000644	33000644	Novel	CCDC7	G159E	476G>A	exon7	628:NP_078964:NM_024688	2	0	2
3	112066521	112066521	Novel	CD200	E180K	538G>A	exon4	269:NP_005935:NM_005944	2	2	0
17	72469704	72469704	Novel	CD300A	V24L	70G>T	exon2	299:NP_009192:NM_007261	2	2	0
9	123230234	123230234	Novel	CDK5RAP2	D670E	2010C>A	exon18	1893:NP_060719:NM_018249	2	2	0
2	233398802	233398802	Novel	CHRND	K403N	1209G>T	exon10	517:NP_000742:NM_000751	2	1	1
12	8612225	8612225	Novel	CLEC6A	K52Q	154A>C	exon3	209:NP_001007034:NM_001007033	2	0	2
18	641356	641356	Novel	CLUL1	E342Q	1024G>C	exon7	466:NP_954636:NM_199167	2	2	0
10	96535245	96535245	Novel	CYP2C19	R144S	430C>A	exon3	490:NP_000760:NM_000769	2	1	1
14	73425415	73425415	Novel	DCAF4	P464S	1390C>T	exon14	495:NP_056419:NM_015604	2	2	0
9	1056381	1056381	Novel	DMRT2	A265D	794C>A	exon4	561:NP_870987:NM_181872	2	2	0
10	70182518	70182518	Novel	DNA2	R780W	2338C>T	exon15	1060:NP_001073918:NM_001080449	2	1	1
16	84188196	84188196	Novel	DNAAF1	E123K	367G>A	exon4	725:NP_848547:NM_178452	2	2	0
20	35399515	35399515	Novel	DSN1	S39F	116C>T	exon3	356:NP_079194:NM_024918	2	2	0
8	27957346	27957346	Novel	ELP3	V41M	121G>A	exon3	547:NP_060561:NM_018091	2	2	0
10	119307652	119307652	Novel	EMX2	Q223L	668A>T	exon3	252:NP_004089:NM_004098	2	2	0
11	6232756	6232756	Novel	FAM160A2	C981R	2941T>C	exon12	986:NP_115503:NM_032127	2	2	0

Chr	Start (hg19)	End (hg19)	Gene Status	Gene	AA Change	cdna change	Exon	LongRef_Details	FALS_index_hets	Discovery	Replication
2	242431003	242431003	Novel	FARP2	G899E	2696G>A	exon24	1054:NP_055623:NM_014808	2	2	0
3	13679370	13679370	Novel	FBLN2	T1169I	3506C>T	exon17	1184:NP_001989:NM_001998	2	2	0
4	155505337	155505337	Novel	FGA	R847K	2540G>A	exon6	866:NP_000499:NM_000508	2	2	0
1	27942290	27942290	Novel	FGR	G250S	748G>A	exon8	529:NP_005239:NM_005248	2	2	0
12	8196678	8196678	Novel	FOXJ2	S203R	609C>G	exon5	574:NP_060886:NM_018416	2	1	1
1	74670585	74670585	Novel	FPGT	L298R	893T>G	exon4	594:NP_003829:NM_003838	2	2	0
10	35929469	35929469	Novel	FZD8	S297T	889T>A	exon1	694:NP_114072:NM_031866	2	2	0
10	35929468	35929468	Novel	FZD8	S297F	890C>T	exon1	694:NP_114072:NM_031866	2	2	0
4	47427769	47427769	Novel	GABRB1	V387M	1159G>A	exon9	474:NP_000803:NM_000812	2	2	0
2	233671276	233671276	Novel	GIGYF2	A593V	1778C>T	exon17	1320:NP_001096617:NM_001103147	2	1	1
12	133353644	133353644	Novel	GOLGA3	A1252V	3755C>T	exon20	1498:NP_005886:NM_005895	2	2	0
12	14834362	14834362	Novel	GUCY2C	G221S	661G>A	exon5	1073:NP_004954:NM_004963	2	2	0
1	24144010	24144010	Novel	HMGCL	V70L	208G>C	exon3	325:NP_000182:NM_000191	2	1	1
3	50326753	50326753	Novel	IFRD2	S337I	1010G>T	exon8	506:NP_006755:NM_006764	2	2	0
4	143326459	143326459	Novel	INPP4B	A52G	155C>G	exon7	924:NP_003857:NM_003866	2	2	0
2	160968716	160968716	Novel	ITGB6		1568-6C>G	exon13	na	2	1	1
19	54871655	54871655	Novel	LAIR1	P130L	389C>T	exon4	287:NP_002278:NM_002287	2	1	1
5	154173227	154173227	Novel	LARP1	R194H	581G>A	exon5	1019:NP_056130:NM_015315	2	1	1
15	101550975	101550975	Novel	LRRK1	S405F	1214C>T	exon9	2015:NP_078928:NM_024652	2	2	0
11	24750759	24750759	Novel	LUZP2	K36R	107A>G	exon2	346:NP_001009909:NM_001009909	2	2	0
X	151092183	151092183	Novel	MAGEA4	V16A	47T>C	exon3	317:NP_002353:NM_002362	2	2	0
1	118009038	118009038	Novel	MAN1A2	R386H	1157G>A	exon8	641:NP_006690:NM_006699	2	1	1
13	113743978	113743978	Novel	MCF2L	D963E	2889C>A	exon26	1125:NP_001106203:NM_001112732	2	0	2
22	20939211	20939211	Novel	MED15	V585I	1753G>A	exon14	748:NP_056973:NM_015889	2	1	1
7	100839620	100839620	Novel	MOGAT3	L240R	719T>G	exon6	341:NP_835470:NM_178176	2	2	0
11	60291368	60291368	Novel	MS4A13		130-2A>T	exon4	112:NP_001094379:NM_001100909	2	2	0
16	70712181	70712181	Novel	MTSS1L	F200V	598T>G	exon8	747:NP_612392:NM_138383	2	2	0
1	148252811	148252811	Novel	NBPF14	K2712I	8135A>T	exon65	921:NP_056198:NM_015383	2	2	0
1	148591281	148591281	Novel	NBPF15	D449A	1346A>C	exon15	670:NP_775909:NM_173638	2	2	0
19	15292547	15292547	Novel	NOTCH3	G878R	2632G>C	exon17	2321:NP_000426:NM_000435	2	1	1
10	45799147	45799147	Novel	OR13A1	S242G	724A>G	exon4	328:NP_001004297:NM_001004297	2	1	1
14	20482665	20482665	Novel	OR4K14	A230P	688G>C	exon1	310:NP_001004712:NM_001004712	2	2	0
11	6191099	6191099	Novel	OR52B2	R153Q	458G>A	exon1	323:NP_001004052:NM_001004052	2	0	2
1	36884605	36884605	Novel	OSCP1	I337T	1010T>C	exon9	379:NP_659484:NM_145047	2	0	2
12	121666658	121666658	Novel	P2RX4	M246V	736A>G	exon7	388:NP_002551:NM_002560	2	2	0
12	103306691	103306691	Novel	PAH		61-15C>A	exon3	452:NP_000268:NM_000277	2	1	1
8	22447189	22447189	Novel	PDLIM2	R483L	1448G>T	exon8	602:NP_067643:NM_021630	2	0	2
11	17167247	17167247	Novel	PIK3C2A	H558Y	1672C>T	exon7	1686:NP_002636:NM_002645	2	2	0
21	46697019	46697019	Novel	POFUT2	E248D	744G>C	exon6	429:NP_598368:NM_133635	2	1	1
10	45484756	45484756	Novel	RASSF4	T189I	566C>T	exon7	321:NP_114412:NM_032023	2	2	0
18	20573246	20573246	Novel	RBBP8	V486M	1456G>A	exon11	897:NP_976036:NM_203291	2	2	0
17	6917595	6917595	Novel	RNASEK	M135K	404T>A	exon3	137:NP_001004333:NM_001004333	2	2	0
18	13731682	13731682	Novel	RNMT	A56T	166G>A	exon3	476:NP_003790:NM_003799	2	2	0
14	94915009	94915009	Novel	SERPINA11	P35T	103C>A	exon2	422:NP_001073920:NM_001080451	2	2	0

Chr	Start (hg19)	End (hg19)	Gene Status	Gene	AA Change	cdna change	Exon	LongRef_Details	FALS_index_hets	Discovery	Replication
19	4362692	4362692	Novel	SH3GL1	P257R	770C>G	exon8	368:NP_003016:NM_003025	2	2	0
8	145153884	145153884	Novel	SHARPIN	C354Y	1061G>A	exon8	387:NP_112236:NM_030974	2	2	0
9	94809966	94809966	Novel	SPTLC1	A305T	913G>A	exon10	473:NP_006406:NM_006415	2	2	0
1	47737850	47737850	Novel	STIL	D761N	2281G>A	exon13	1288:NP_001041631:NM_001048166	2	1	1
22	24580184	24580184	Novel	SUSD2	T174A	520A>G	exon4	822:NP_062547:NM_019601	2	2	0
3	33249395	33249395	Novel	SUSD5	S105N	314G>A	exon3	629:NP_056366:NM_015551	2	2	0
16	71602673	71602673	Novel	TAT	D389N	1165G>A	exon11	454:NP_000344:NM_000353	2	1	1
6	46660378	46660378	Novel	TDRD6	I1505V	4513A>G	exon1	2096:NP_001010870:NM_001010870	2	2	0
8	42693473	42693473	Novel	THAP1	D92Y	274G>T	exon3	213:NP_060575:NM_018105	2	1	1
3	156396031	156396031	Novel	TIPARP	I182T	545T>C	exon2	657:NP_056323:NM_015508	2	2	0
2	171974346	171974346	Novel	TLK1	S54T	161G>C	exon2	766:NP_036422:NM_012290	2	0	2
17	42092217	42092217	Novel	TMEM101	L35P	104T>C	exon1	257:NP_115752:NM_032376	2	1	1
9	74360477	74360477	Novel	TMEM2	D164G	491A>G	exon4	1383:NP_037522:NM_013390	2	2	0
17	7572979	7572979	Novel	TP53	T377I	1130C>T	exon11	393:NP_000537:NM_000546	2	0	2
16	1306562	1306562	Novel	TPSD1	E43G	128A>G	exon2	242:NP_036349:NM_012217	2	0	2
16	1306564	1306564	Novel	TPSD1	A44P	130G>C	exon2	242:NP_036349:NM_012217	2	0	2
2	178417073	178417073	Novel	TTC30B	P140Q	419C>A	exon1	665:NP_689730:NM_152517	2	1	1
19	17758154	17758154	Novel	UNC13A	A655V	1964C>T	exon16	1703:NP_001073890:NM_001080421	2	2	0
19	17716941	17716941	Novel	UNC13A	D1678E	5034C>A	exon42	1703:NP_001073890:NM_001080421	2	2	0
9	96030059	96030059	Novel	WNK2	R1243Q	3728G>A	exon16	2217:NP_006639:NM_006648	2	2	0
10	286903	286903	Novel	ZMYND11	Y275F	824A>T	exon9	602:NP_006615:NM_006624	2	2	0
12	133780923	133780923	Novel	ZNF268	R884I	2651G>T	exon6	947:NP_003406:NM_003415	2	2	0
17	18566459	18566459	Novel	ZNF286B	S120R	360C>A	exon5	522:NP_001138517:NM_001145045	2	2	0

Supplementary Table 2. All ANXA11 variants found in index FALS and SALS cases with control frequencies, including exome depth and coverage information

Genomic Position	Ref	Var	Exon	Change	cDNA	Amino Acid	Novelty	FALS Index Hets	All FALS>10x	ALL FALS Av Depth	KCL Hets	dbSNP142	1000 Genomes	Italian Control Exomes (n=3596)	Italian Control Exomes Av Depth	UK10K (n=3781)	EVS_EU_Coverage	EVS EU Hets	ExAC_ALL	ExAC (EU)	ALSDB	SIFT	Polyphen
81932595	G	A	4	Nonsynon	23C>T	P8L	na	8	880	78	9	rs147334030	0.0021965			53	4300	67	870	758	15	T:0.03	D:1.0
81930615	C	T	5	Nonsynon	112G>A	G38R	na	2	877	73	0	rs142083484	0	0	89	1	4300	1	6	5	0	D:0.01	D:1.0
81930608	T	C	5	Nonsynon	119A>G	D40G	NOVEL	3	878	75	0	na	0	0	89	0	4300	0	None	None	0	T:0.78	D:0.996
81929047	GCCCCAGGG	-	6	Non-fshift deletion	231_239del	77_80del	na	0	562	18	0	na	0			0	4228	0	10	0	0	na	na
81929022	G	A	6	Synon	264C>T	G88G	na	1	575	16	0	rs138254262	0.0009984			0	4169	1	32	3	0	D:0	na
81928983	A	G	6	Syno	303T>C	P101P	na	27	674	16	14	rs11542746	0.0031949			160	4207	102	1142	955	46	na	na
81928963	G	A	6	Nonsynon	323C>T	P108L [#]	na	0	701	17	0	na	0	0		0	4245	0	None	None	0	T:0.64	T:0.92
81928915	G	A	6	Nonsynon	371C>T	P124L [#]	na	1	715	22	0	na	0			0	4258	0	2	1	0	D:0.01	D:0.994
81928830	G	A	6	Synon	456C>T	Y152Y	na	26	762	40	12	rs34003188	0.0087859			99	4295	155	1269	964	36	na	na
81928812	C	A	6	Synon	474G>T	V158V	na	3	774	45	1	rs139412104	0.0019968			8	4293	22	183	143	6	na	na
81928763	C	T	6	Nonsynon	523G>A	G175R	NOVEL	1	745	38	0	na	0	0	19	0	4291	0	0	None	1	T:0.11	T:0.005
81927065	C	T	7	Nonsynon	566G>A	G189E*	na	0	864	50	na	rs569546089	0	1	63	0	4300	0	17	14	1	T:0.18	D:0.999
81927059	C	T	7	Nonsynon	572G>A	R191Q	na	86	863	53	80	rs2229554	0.0219649			521	4300	547	6073	4702	202	T:0.48	D:1.0
81927002	C	T	7	Nonsynon	629G>A	R210Q	na	1	876	67	3	rs147610631	0.0013978			5	4300	12	138	72	1	D:0.01	D:0.995
81926736	C	T	8	Synon	654G>A	T218T	na	1	825	61	0	rs200066001	0			0	4300	0	6	5	0	na	na
81926718	A	G	8	Synon	672T>C	I224I	na	173	836	76	134	rs2228427	0.108427			1019	4300	1063	15140	8078	343	na	na
81926702	G	A	8	Nonsynon	688C>T	R230C	na	357	837	85	268	rs1049550	0.392173			3157	4300	2041	45030	24922	649	D:0.01	D:1.0
81926686	C	T	8	Nonsynon	704G>A	R235Q	NOVEL	0	836	94	na	na	0	0	22	0	4300	0	0	0	0	D:0	D:1.0
81926659	G	A	8	Nonsynon	731C>T	T244M	na	3	824	90	3	rs41310298	0.0017971			22	4300	30	203	175	9	D:0	D:1.0
81925945	G	T	9	Synon	753C>A	I251I	NOVEL	0	876	59	0	na	0			0	4300	0	None	None	0	na	na
81925903	T	C	9	Synon	795A>G	T265T	na	1	882	81	0	rs150935845	0			1	4300	6	17	14	0	na	na
81925902	T	C	9	Nonsynon	796A>G	I266V	na	0	882	81	0	na	0			0	4300	0	1	0	0	T:0.33	T:0.284
81925866	T	C	9	Nonsynon	832A>G	I278V	na	7	879	72	8	rs72807973	0.0023962			33	4300	42	363	281	20	T:0.15	T:0.018
81923347	C	T	11	Synon	972G>A	E324E	na	1	825	93	0	rs146139449	0			0	4287	1	1	1	0	na	na
81923155	G	A	12	Nonsynon	1036C>T	R346C	NOVEL	1	883	108	0	na	0	0	58	0	4300	0	0	None	0	D:0	D:1.0
81921766	C	T	13	Nonsynon	1105G>A	E369K	na	5	827	56	4	rs34414015	0.0017971			42	4300	50	488	400	14	D:0	D:1.0
81918880	G	A	14	Synon	1252C>T	L418L	na	3	874	71	0	rs61860018	0.0001997			5	4300	10	46	42	3	na	na
81917486	T	C	16	Nonsynon	1369A>G	I457V	na	13	885	95	8	rs1802932	0.0033946			94	4300	103	1086	764	43	T:0.32	T:0.409
81917463	G	A	16	Synon	1392C>T	T464T	na	1	887	106	0	rs374382845	0			1	4300	1	4	3	0	na	na

Supplementary Table 3. Clinical details of patients with ANXA11 mutations.

Patient	Cohort	Mutation	Gender	FALS / SALS	Age of onset (years)	Site of onset (Limb / Bulbar)	Disease Duration (months)	FTD (Y/N)
Patient 1 F1 III:2	Discovery	p.D40G	F	FALS	74	BULBAR	60	N
Patient 2 F2 III:19	Discovery	p.D40G	F	FALS	70	LIMB	72	N
Patient 3	Replication	p.D40G	F	FALS	55	BULBAR	-	N
Patient 4 F1 III:5	Discovery	p.D40G	F	FALS	72	BULBAR	-	N
Patient 5 F2 II:2	Discovery	p.D40G	M	FALS	83	BULBAR	24	N
Patient 6	Discovery	p.G38R	M	FALS	50	MIXED	12	N
Patient 7	Discovery	p.G38R	M	FALS	62	LIMB	ALIVE	N
Patient 8	Replication	p.G175R	M	FALS	61	LIMB	-	N
Patient 9	Replication	p.R346C	M	FALS	74	LIMB	181	N
Patient 10	Sporadic	p.D40G	M	SALS	72	BULBAR	36	N
Patient 11	Sporadic	p.G189E	M	SALS	53	LIMB	24	N
Patient 12	Sporadic	p.R235Q	F	SALS	65	BULBAR	24	N

Figure 1. *Annexin A11* mutations identified in ALS patients following stringent filtering of exome sequencing data.

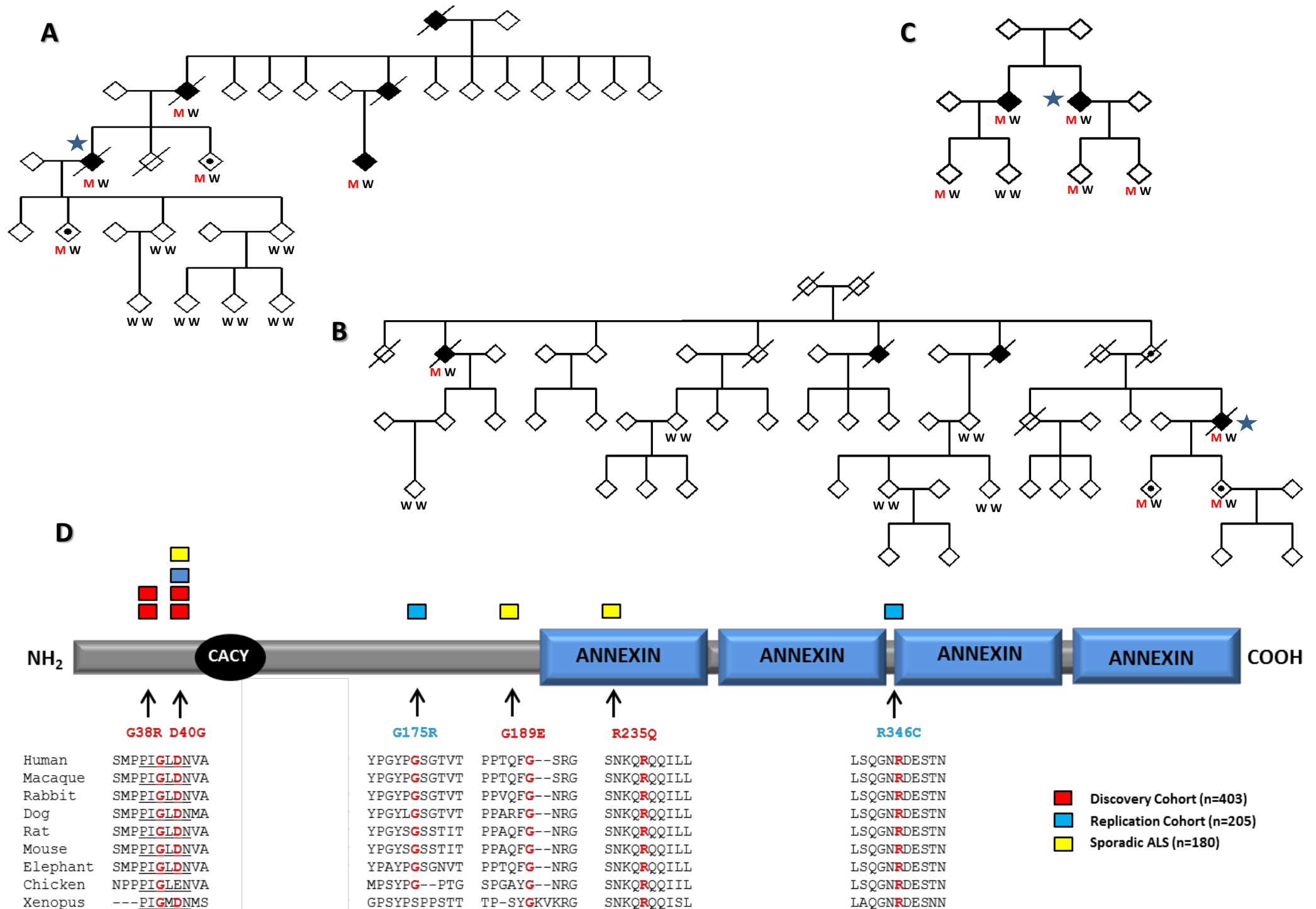
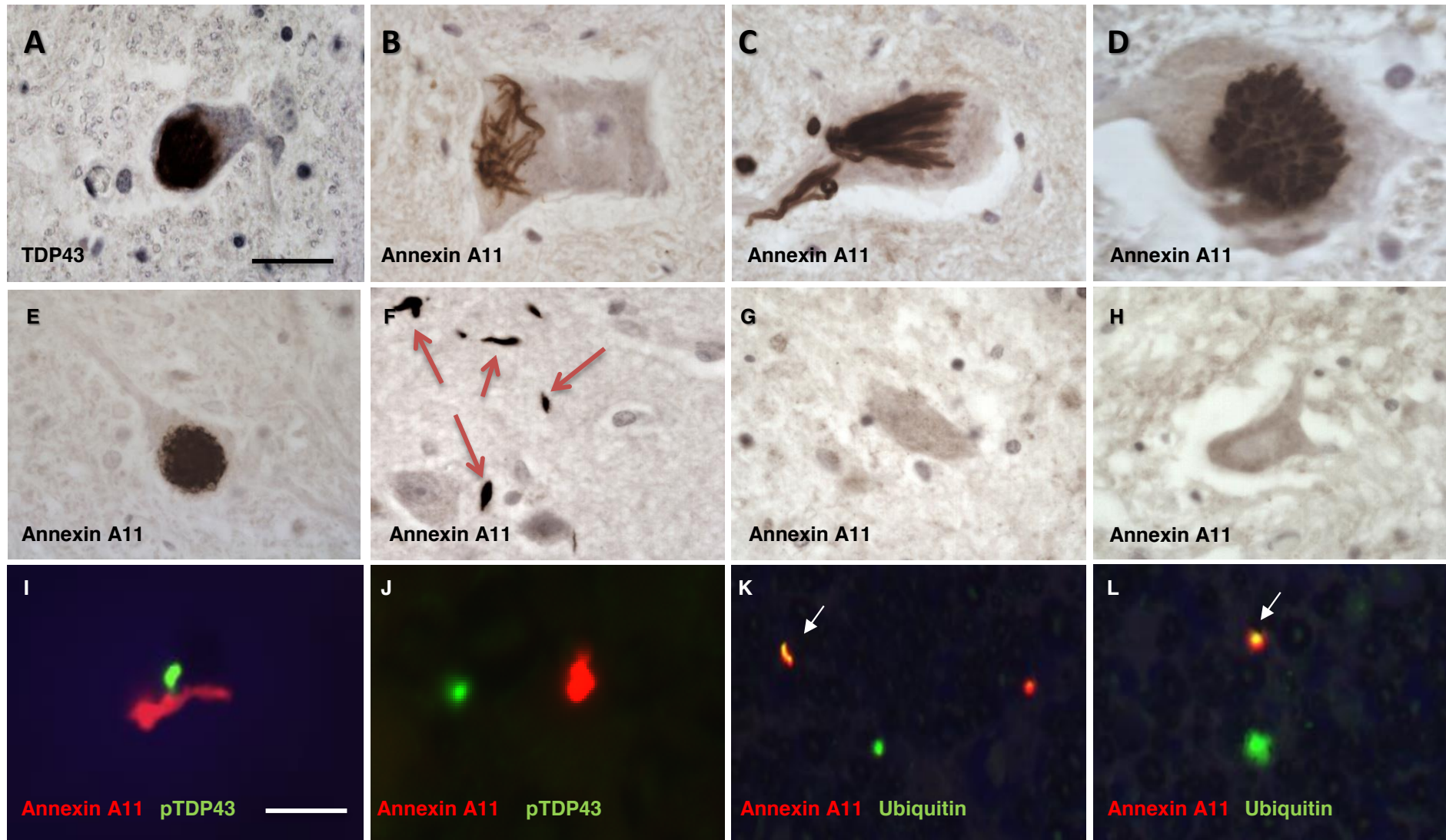
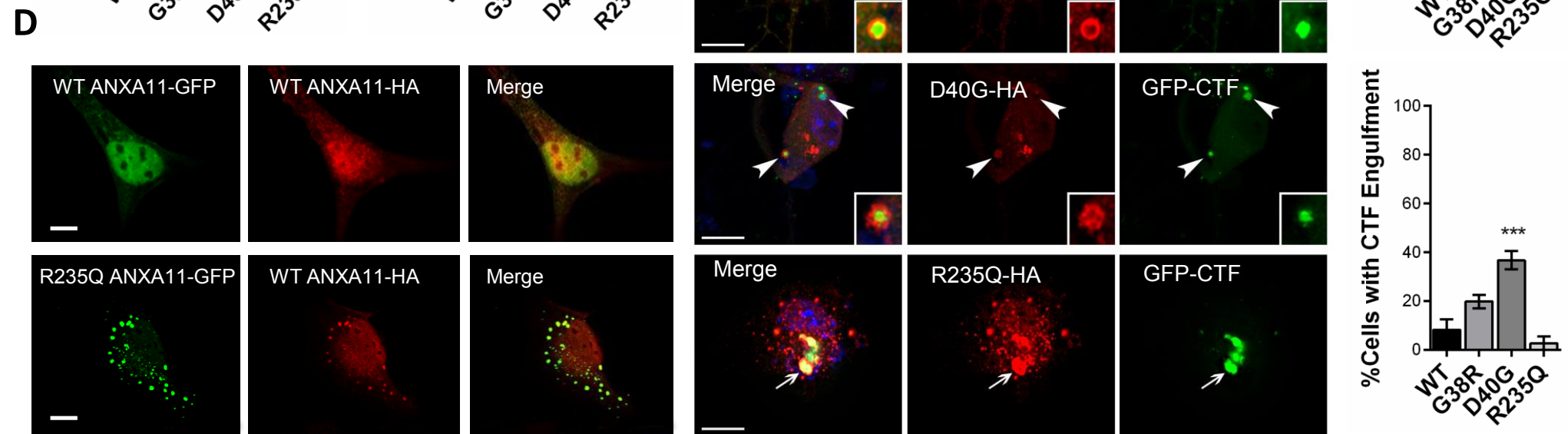
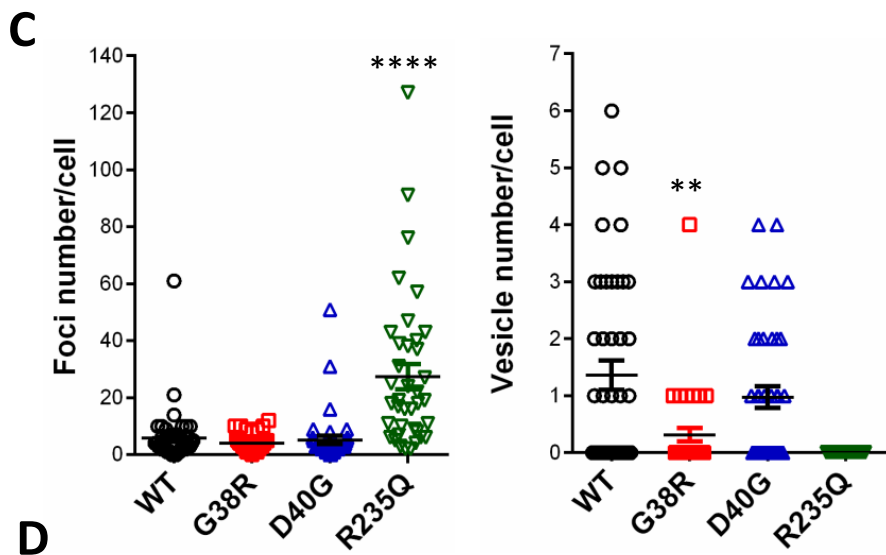
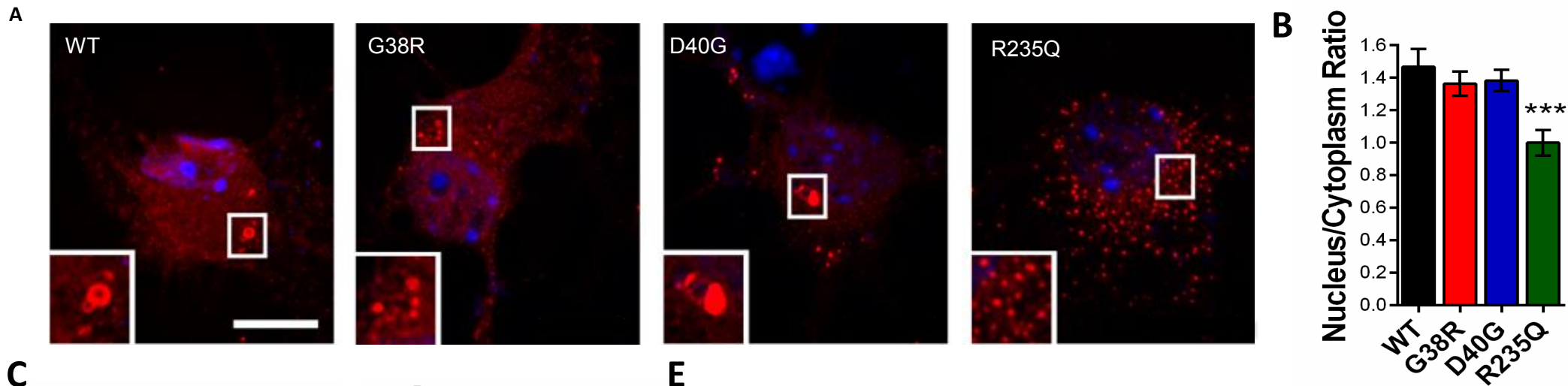
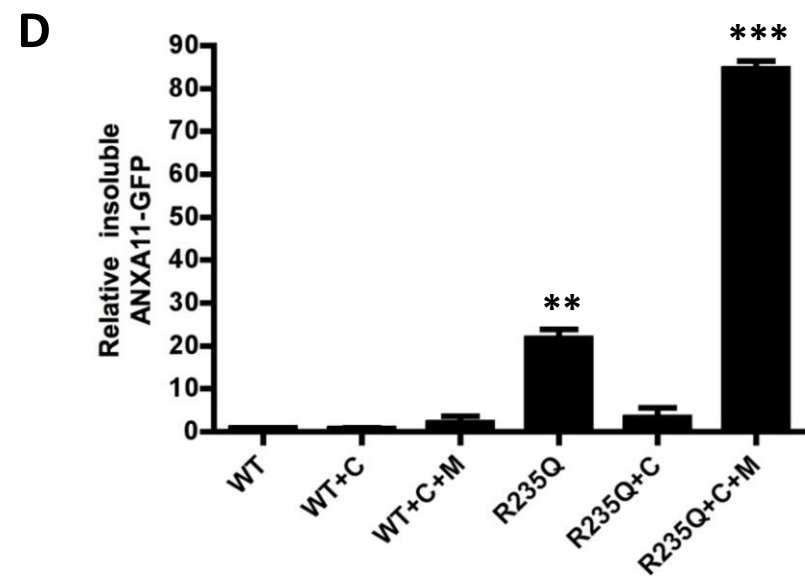
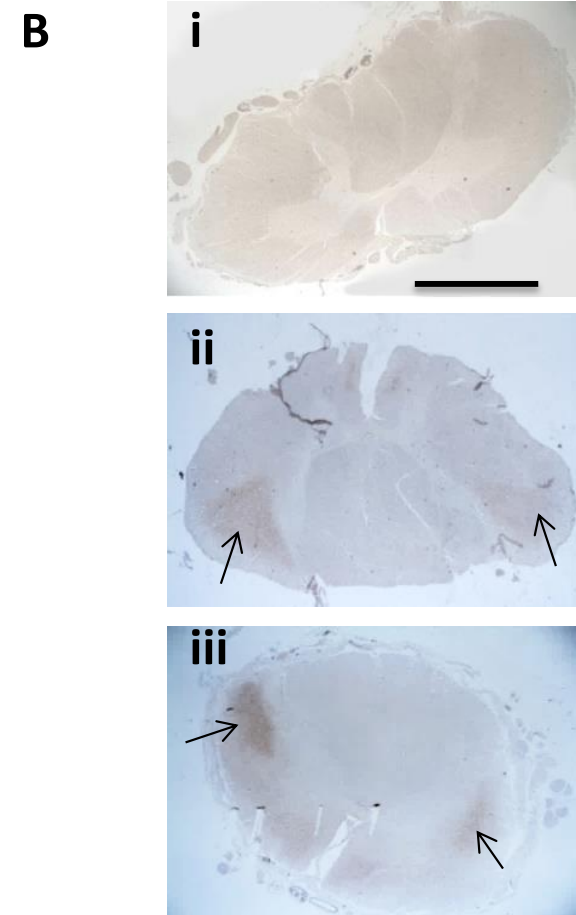
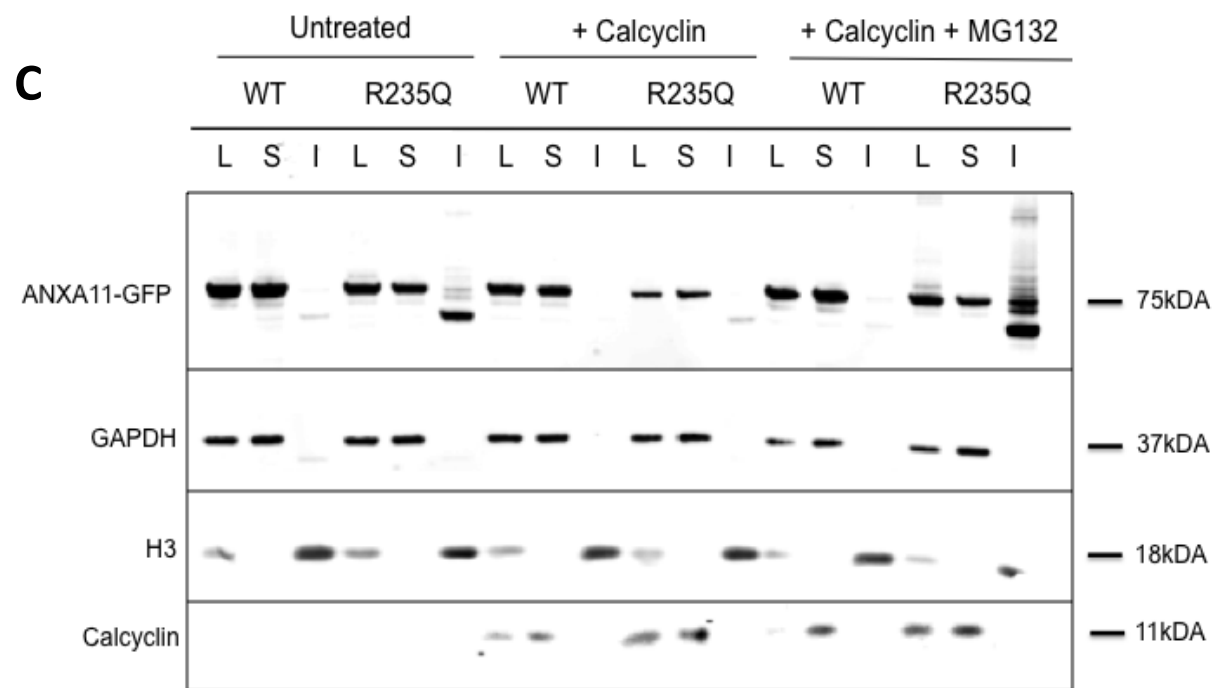
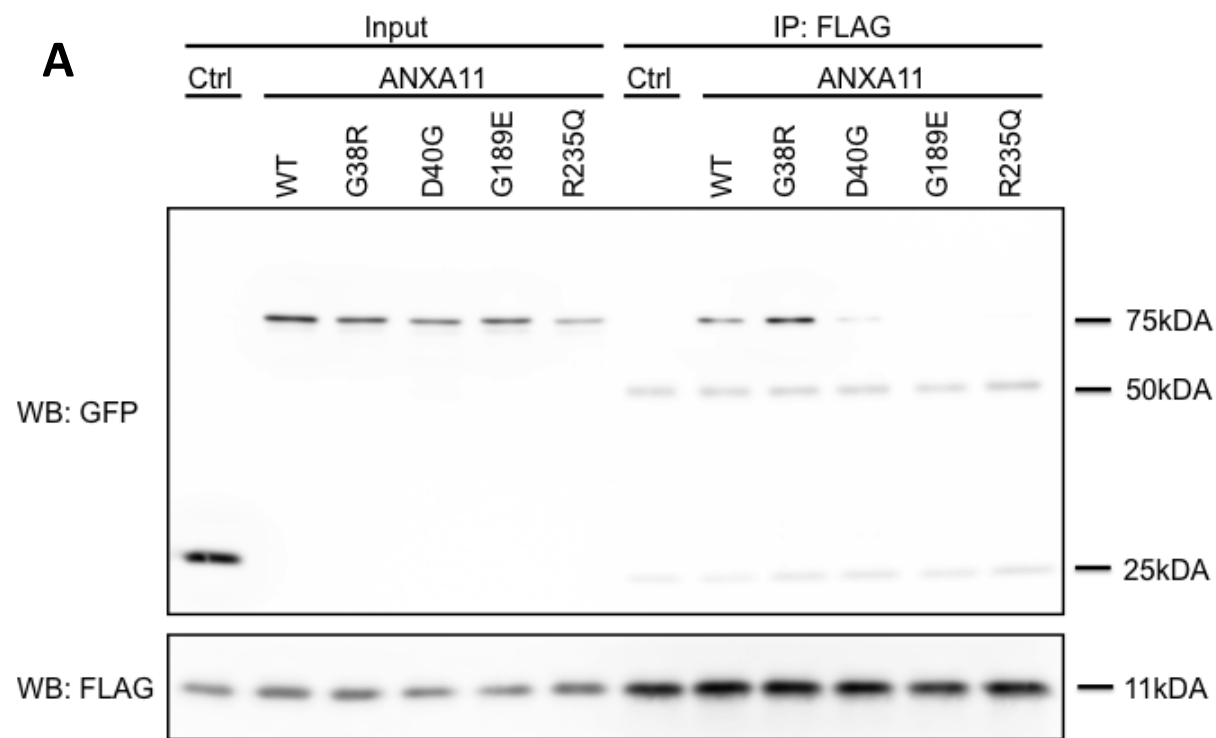


Figure 2. TDP-43 and Annexin A11 immunohistochemistry from post-mortem spinal cord tissue of a SALS case harbouring the novel D40G mutation.





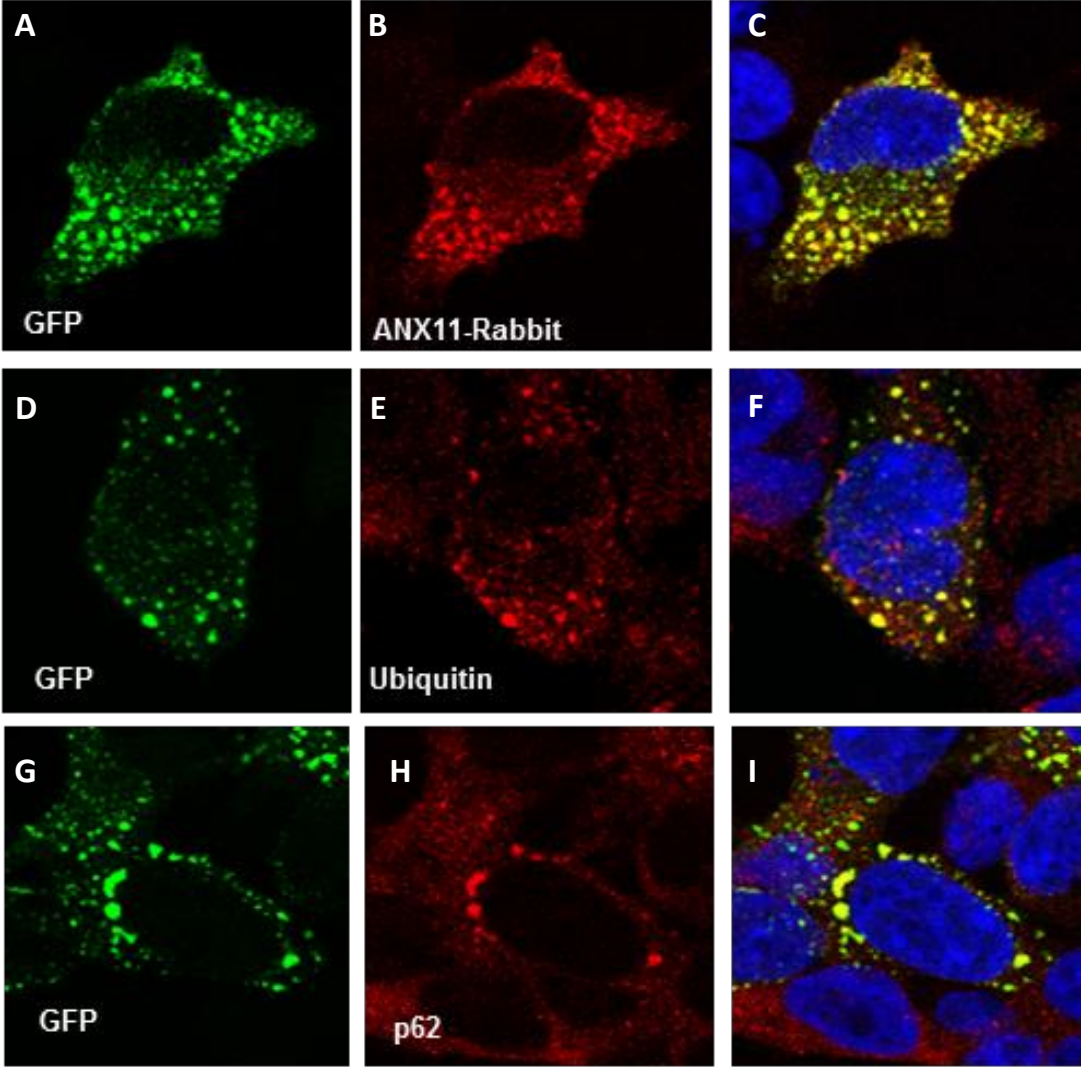


Supplementary Figure 1.

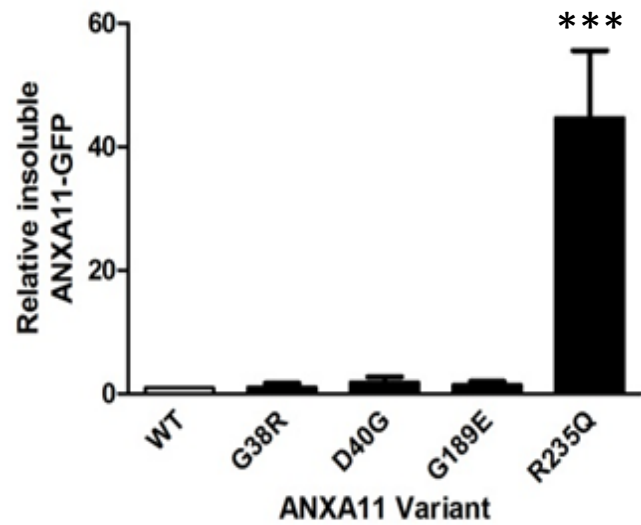
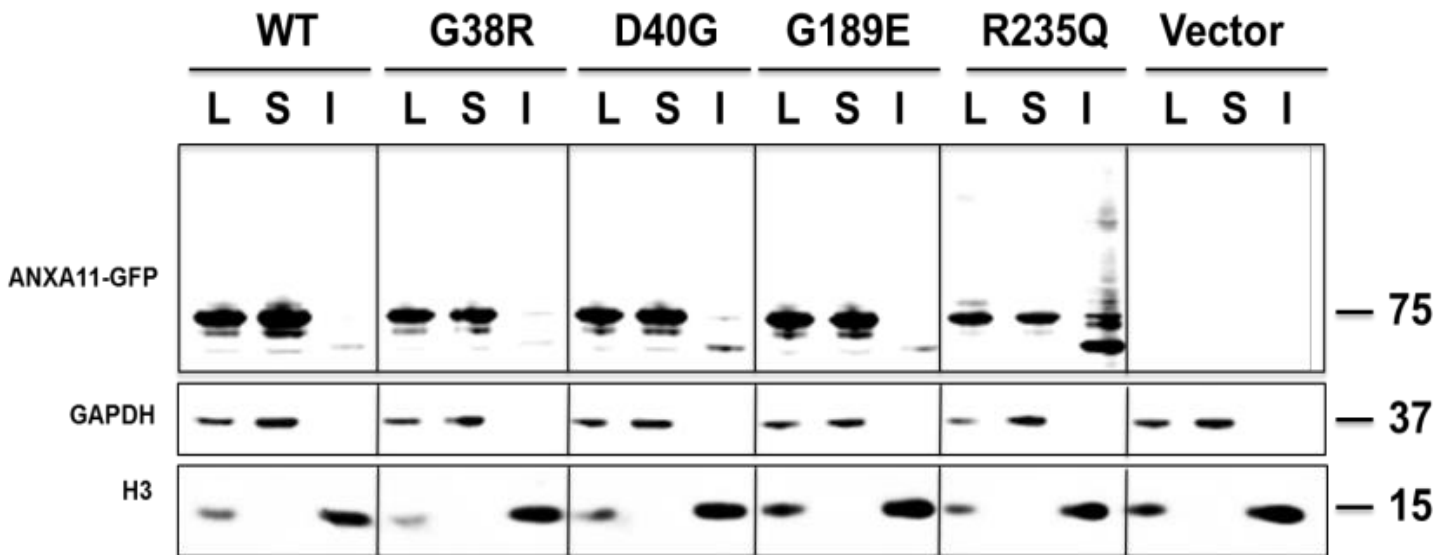
The *Annexin A11* p.D40G mutation shares a common haplotype comprised of 8 SNPs and 2 microsatellites.

Marker	Position (Ch 10)	Change	MAF	FAMILY 1 – D40G				FAMILY 2 – D40G				D40G Sporadic		G38R		G38R	
				Individual III:2	Individual III:5	Individual II:2	Individual II:19	Patient 10	Patient 6	Patient 7							
rs185034903	82007218	C>T	0.07	C	T	C	T	C	T	C	T	C	T	C	C	C	C
rs148817640	82005957	C>G	0.07	C	G	C	G	C	G	C	G	C	G	C	C	C	C
Micro1	81991564	(TTG)n	na	303	312	303	312	306	312	303	312	306	312	300	306	303	324
rs11202162	81977939	C>A	0.09	C	A	C	A	C	A	C	A	C	A	C	C	C	C
rs73299551	81955112	A>G	0.107	A	G	A	G	A	G	A	G	A	G	A	A	A	A
Micro2	81947737	(AT)n	na	208	196	208	196	180	196	212	196	200	196	186	186	196	216
ANXA11 A>G	81930608	A>G	Novel	A	G	A	G	A	G	A	G	A	G	A	A	A	A
rs41310300	81926538	C>T	0.12	C	T	C	T	C	T	C	T	C	T	C	C	C	C
rs73299508	81912409	G>C	0.12	G	C	G	C	G	C	G	C	G	C	G	G	G	C
rs2184702	81906299	T>G	0.11	T	G	T	G	T	G	T	G	T	G	G	G	T	G
rs41291392	81904645	C>T	0.11	C	T	C	T	C	T	C	T	C	T	C	C	C	C

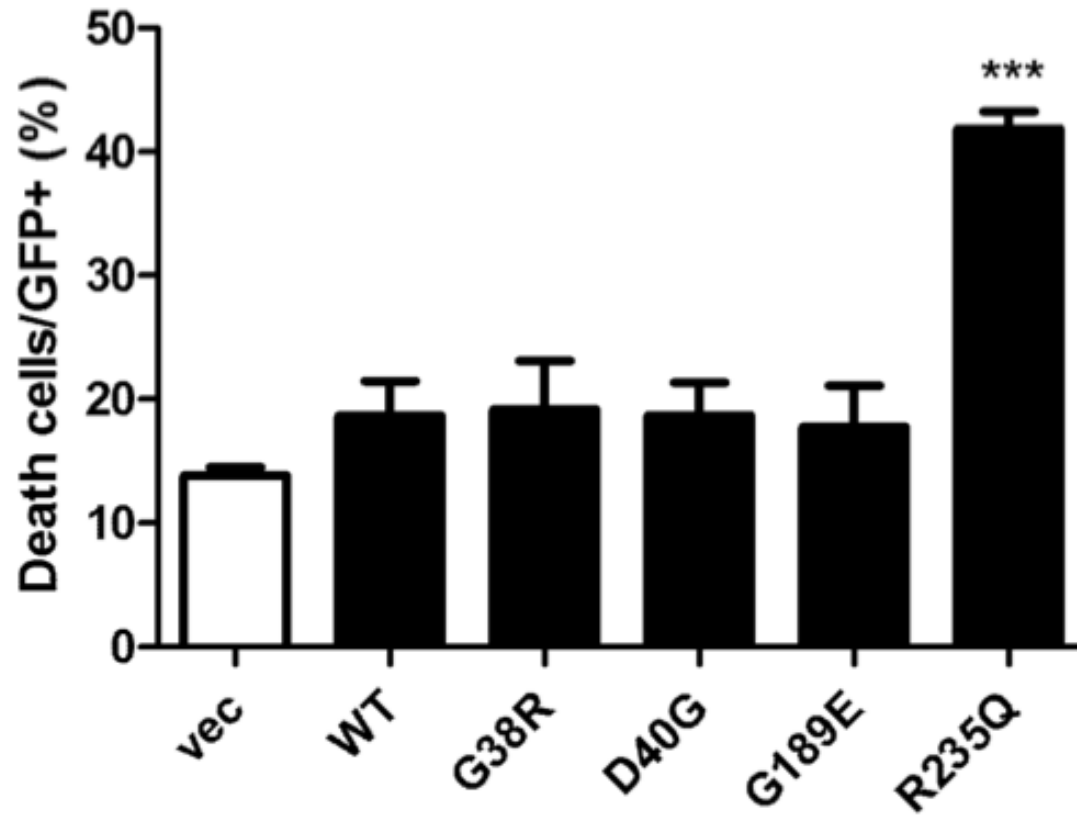
Supplementary Figure 2. R235Q ANXA11-GFP co-localises with ubiquitin and p62 in HEK cells.



Supplementary Figure 3 – R235Q ANXA11-GFP forms high molecular weight detergent resistant aggregates in HEK cells



Supplementary Figure 4. Cell survival assay of ANXA11-GFP WT and mutant constructs shows R235Q to be toxic in SH-SH5Y cells



Supplementary Figure 6. N-terminal Annexin A11 mutations do not alter binding of Sorcin and ALG2.

